

# UC San Diego

## UC San Diego Previously Published Works

### Title

A Critical Role for DLK and LZK in Axonal Repair in the Mammalian Spinal Cord.

### Permalink

<https://escholarship.org/uc/item/8hw893ct>

### Journal

Journal of Neuroscience, 42(18)

### ISSN

0270-6474

### Authors

Saikia, Junmi M  
Chavez-Martinez, Carmine L  
Kim, Noah D  
[et al.](#)

### Publication Date



2022-05-04

### DOI

10.1523/jneurosci.2495-21.2022

Peer reviewed

# A Critical Role for DLK and LZK in Axonal Repair in the Mammalian Spinal Cord

Junmi M. Saikia,<sup>1,2</sup> Carmine L. Chavez-Martinez,<sup>1,3</sup> Noah D. Kim,<sup>1</sup> Sahar Allibhoy,<sup>1</sup> Hugo J. Kim,<sup>1</sup> Lidiya Simonyan,<sup>1</sup> Samraa Smadi,<sup>1</sup> Kristen M. Tsai,<sup>1</sup>  Daniel Romaus-Sanjurjo,<sup>1</sup> Yishi Jin,<sup>1,4,5</sup> and  Binhai Zheng<sup>1,6</sup>

<sup>1</sup>Department of Neurosciences, School of Medicine, <sup>2</sup>Neurosciences Graduate Program, <sup>3</sup>Graduate Program in Biological Sciences, <sup>4</sup>Department of Neurobiology, School of Biological Sciences, <sup>5</sup>Department of Cellular and Molecular Medicine, School of Medicine, University of California San Diego, La Jolla, California 92093, and <sup>6</sup>VA San Diego Healthcare System Research Service, San Diego, California 92161

The limited ability for axonal repair after spinal cord injury underlies long-term functional impairment. Dual leucine-zipper kinase [DLK; MAP kinase kinase kinase 12; MAP3K12] is an evolutionarily conserved MAP3K implicated in neuronal injury signaling from *Caenorhabditis elegans* to mammals. However, whether DLK or its close homolog leucine zipper kinase (LZK; MAP3K13) regulates axonal repair in the mammalian spinal cord remains unknown. Here, we assess the role of endogenous DLK and LZK in the regeneration and compensatory sprouting of corticospinal tract (CST) axons in mice of both sexes with genetic analyses in a regeneration competent background provided by PTEN deletion. We found that inducible neuronal deletion of both DLK and LZK, but not either kinase alone, abolishes PTEN deletion-induced regeneration and sprouting of CST axons, and reduces naturally-occurring axon sprouting after injury. Thus, DLK/LZK-mediated injury signaling operates not only in injured neurons to regulate regeneration, but also unexpectedly in uninjured neurons to regulate sprouting. Deleting DLK and LZK does not interfere with PTEN/mTOR signaling, indicating that injury signaling and regenerative competence are independently controlled. Together with our previous study implicating LZK in astrocytic reactivity and scar formation, these data illustrate the multicellular function of this pair of MAP3Ks in both neurons and glia in the injury response of the mammalian spinal cord.

## Significance Statement

Functional recovery after spinal cord injury is limited because of a lack of axonal repair in the mammalian CNS. Dual leucine-zipper kinase (DLK) and leucine zipper kinase (LZK) are two closely related protein kinases that have emerged as regulators of neuronal responses to injury. However, their role in axonal repair in the mammalian spinal cord has not been described. Here, we show that DLK and LZK together play critical roles in axonal repair in the mammalian spinal cord, validating them as potential targets to promote repair and recovery after spinal cord injury. In addition to regulating axonal regeneration from injured neurons, both kinases also regulate compensatory axonal growth from uninjured neurons, indicating a more pervasive role in CNS repair than originally anticipated.

Received Dec. 19, 2021; revised Feb. 23, 2022; accepted Mar. 24, 2022.

Author contributions: J.M.S., N.D.K., Y.J., and B.Z. designed research; J.M.S., C.L.C.-M., N.D.K., S.A., L.S., S.S., K.M.T., and B.Z. performed research; Y.J. and B.Z. contributed unpublished reagents/analytic tools; J.M.S., C.L.C.-M., N.D.K., S.A., H.J.K., D.R.-S., and B.Z. analyzed data; J.M.S. and B.Z. wrote the first draft of the paper; J.M.S., C.L.C.-M., H.J.K., D.R.-S., Y.J., and B.Z. edited the paper.

This work was supported by National Institutes of Health/National Institute of Neurological Disorders and Stroke Grants NS093055 and NS047101 (microscopy imaging), the United States Department of Veterans Affairs Grant RX002483, and Wings for Life and Craig H. Neilsen (316915, 733544) foundations. Viral preps were obtained from Boston Children's Hospital Viral Core (EY012196). We thank Geneva Q. Le for help with genotyping and maintenance of mouse lines, Erin Ritchie for her intellectual input regarding BaseScope methods, Juliet Suen for help with perfusions, and Jeffrey Li for his initial involvement with imaging and quantifications.

D. Romaus-Sanjurjo's present address: NeuroAging Group (NEURAL), Clinical Neurosciences Research Laboratories (LINC), Health Research Institute of Santiago de Compostela (IDIS), Santiago de Compostela 15706, Spain.

The authors declare no competing financial interests.

Correspondence should be addressed to Binhai Zheng at [bizheng@health.ucsd.edu](mailto:bizheng@health.ucsd.edu).

<https://doi.org/10.1523/JNEUROSCI.2495-21.2022>

Copyright © 2022 the authors

## Introduction

Within the mammalian CNS, two mechanisms of axonal repair are studied extensively: regeneration from injured neurons, which is generally a non-spontaneous event, or sprouting from uninjured neurons, which occurs spontaneously to some degree after injury (Tuszynski and Steward, 2012; Geoffroy and Zheng, 2014). Axonal regeneration represents the “holy grail” of neural repair, and is important for functional recovery after severe and especially complete spinal cord injury. On the other hand, axonal sprouting can also lead to new connections with target neurons beyond the injury site and contribute to functional recovery but only after incomplete injury. Indeed, even clinically (i.e., neurologically) complete spinal cord injuries are rarely anatomically complete (Angeli et al., 2014), leaving surviving axonal populations that may underlie functional improvement via sprouting or

other forms of plasticity (Sofroniew, 2018). Furthermore, animal studies have illustrated that even spontaneous sprouting may result in intraspinal rewiring, leading to partial recovery of function (Weidner et al., 2001; Bareyre et al., 2004; Ueno et al., 2012).

Limited axonal repair after CNS injury has been attributed to both neuron extrinsic and intrinsic factors. While earlier studies emphasized extrinsic factors such as glial inhibitors of axonal growth (Silver et al., 2014), recent studies highlighted the importance of neuron-intrinsic control of regeneration (He and Jin, 2016). In addition, growth factors are employed extensively to promote axonal repair, especially in the context of cell transplantation (Lu et al., 2012). A key neuron-intrinsic inhibitor of axonal regeneration identified was PTEN, deletion of which enhances the regeneration of retinal and corticospinal tract (CST) axons (Park et al., 2008; Liu et al., 2010). PTEN is a negative regulator of the mTOR pathway, which controls protein synthesis and cell growth. Both retinal ganglion cells (RGCs) and corticospinal neurons (also known as corticospinal motor neurons) undergo a development-dependent decline in mTOR activity, which is further downregulated on injury in the adult CNS (Park et al., 2008; Liu et al., 2010). PTEN deletion reverses this decline in mTOR activity, thereby driving cellular metabolism and providing the building blocks required for regeneration. As such, the PTEN/mTOR pathway is considered to regulate the “regenerative competence” of adult CNS neurons (Lu et al., 2014).

Another aspect for the neuron-intrinsic control of axonal repair is injury signaling, as exemplified by the pathway involving dual leucine-zipper kinase (DLK), a mitogen-activated protein kinase kinase kinase (MAP3K). Upon receiving external or internal stimuli, MAP3K, MAP2K, and MAPK undergo a phosphorylation cascade, activating downstream effectors and producing various cellular responses (Chang and Karin, 2001). In the nervous system, the DLK pathway has been implicated in divergent cellular processes, including neuronal development, response to injury, and apoptosis (Tedeschi and Bradke, 2013; Jin and Zheng, 2019). The original identification of DLK and LZK as upstream regulators of MAP3K signaling dates back to the mid-1990s during a period of extensive kinase discovery (Holzman et al., 1994; Sakuma et al., 1997). Early functional studies in *Caenorhabditis elegans* indicate that DLK (or DLK-1) regulates presynaptic development (Nakata et al., 2005). Later, worm DLK was found to be critical for axon regeneration (Hammarlund et al., 2009; Yan et al., 2009). The *Drosophila* DLK homolog, Wallenda, is similarly required for synapse development and axon regeneration (Collins et al., 2006; Xiong et al., 2010).

Two mammalian homologs to invertebrate DLK are expressed in the nervous system: DLK (MAP3K12) and leucine zipper kinase (LZK; or MAP3K13). These homologs share >95% sequence homology within their kinase domains, with significant divergence at their C termini (Yan and Jin, 2012). Of the two kinases, DLK has been well characterized for its role in neuronal responses to injury using sciatic and optic nerve injury models. In the peripheral nervous system (PNS), neuronal DLK deletion reduces axon regeneration after sciatic nerve injury and blocks the conditioning lesion effect where a prior injury enhances the regenerative response following a second injury (Shin et al., 2012). Mechanistically, DLK is required for the retrograde transport of injury signaling phosphorylated-STAT3 (p-STAT3) to the cell body. In the CNS, DLK deletion reduces retinal axon regeneration but increases RGC survival, two seemingly contrasting outcomes, after optic nerve injury (Watkins et al., 2013; Welsbie et al., 2013). Co-deleting DLK and LZK further enhances RGC survival although deleting LZK alone has no effect,

indicating that DLK is the more critical player but LZK partially compensates for the loss of DLK in mediating injury-induced RGC death (Welsbie et al., 2017).

Despite knowledge gained from peripheral and optic nerve injury models, a role for DLK or LZK in axonal repair in the mammalian spinal cord has not been demonstrated. Here, we report a critical neuronal role for DLK and LZK in axon regeneration and sprouting in the mammalian spinal cord using the CST as the experimental system. Together with our previous study implicating LZK in mediating the astrocytic response and scar formation after spinal cord injury (Chen et al., 2018), these results support the hypothesis that the mammalian DLK/LZK pathway mediates the multicellular response to CNS injury.

## Materials and Methods

### Experimental mice

Conditional knock-out (cKO) mice were generated in which exon 2 of the DLK or LZK gene is flanked by loxP sites (Chen et al., 2016, 2018; Li et al., 2021). The DLK conditional allele was generously provided by Lawrence B. Holzman (University of Pennsylvania). In these mice, exposure to Cre-recombinase is expected to generate a null allele. DLK<sup>fl/fl</sup> and LZK<sup>fl/fl</sup> mice were bred to each other to generate DLK<sup>fl/fl</sup>;LZK<sup>fl/fl</sup> mice, as well as to PTEN<sup>fl/fl</sup> to generate DLK<sup>fl/fl</sup>;PTEN<sup>fl/fl</sup>, LZK<sup>fl/fl</sup>;PTEN<sup>fl/fl</sup>, and DLK<sup>fl/fl</sup>;LZK<sup>fl/fl</sup>;PTEN<sup>fl/fl</sup> mice. To test the efficiency of gene deletion in DLK<sup>fl/fl</sup> and LZK<sup>fl/fl</sup> mice, fluorescent BaseScope (ACD Biotechne) was applied using probes designed to target the floxed exon for each gene (described below). Age-matched mice of various combinations of homozygous conditional alleles (e.g., DLK<sup>fl/fl</sup>;LZK<sup>fl/fl</sup>;PTEN<sup>fl/fl</sup>) in C57BL/6 background were injected with AAV-Cre to induce gene deletion in the sensorimotor cortex at six to eight weeks of age. Both males and females were used for each genetic conditions in a ratio of ~1:1. Littermates injected with AAV-GFP served as controls.

### Viruses

AAV2-CAG-Cre and AAV2-CAG-GFP were acquired from Boston Children's Hospital Viral Core (AAV2 is abbreviated as AAV throughout the paper). Viral titer is confirmed using qPCR to be  $0.5 \times 10^{12}$  TU/ml. Viruses were injected to the motor cortex via modified 10- $\mu$ l Hamilton syringe with a fine glass capillary needle affixed at the tip of the syringe using two-part epoxy (details below).

### Surgical procedures

#### AAV injections

Cortical injections of AAV-Cre or AAV-GFP were performed on six- to eight-week-old mice. Surgeons were blinded to genotype of mice during all days of surgery. Animals were anesthetized with ketamine and xylazine injected intraperitoneally (i.p. K/X) dosed at 80–100 and 10 mg/kg, respectively. After anesthesia, mice were shaved at the site of surgery and head fixed to a stereotaxic device (Kopf Instruments). The surgical area was sterilized using 70% alcohol and povidone-iodine swabs. Skin above the skull was cut using a pair of scissors or a number 10 surgical scalpel, and the skin was retracted to reveal bregma. A surgical window was drilled carefully to include the coordinates for three sites of injections.

A 10- $\mu$ l Hamilton syringe with a fine glass capillary needle was loaded with 1.5  $\mu$ l of either AAV-Cre or AAV-GFP and mounted onto the stereotaxic device. Injection coordinates were adapted from previous studies targeting the forelimb innervating area for the pyramidotomy model and the hindlimb innervating area for the dorsal hemisection model (Liu et al., 2010; Geoffroy et al., 2015). The coordinates relative to bregma are as follows in order of injection sequence: for pyramidotomy/sprouting studies, 1.2 mm lateral, 0.5 mm anterior, 1.2 mm lateral, 0.5 mm posterior, 2.2 mm lateral, 0.0 mm anterior; for dorsal hemisection/regeneration studies, 1.4 mm lateral, 0.1 mm posterior, 1.4 mm lateral, 1.1 mm posterior, and 1.0 mm lateral, 0.6 mm posterior. For each injection site, the needle was lowered to a depth of 0.9 mm and then raised by 0.2 mm for a final depth of 0.7 mm. The brain was allowed to recover from needle insertion for 2 min. Virus was then delivered at a rate of

0.1  $\mu$ l/min for 4 min, for a total volume of 0.4  $\mu$ l per injection site, and then virus was given time to diffuse into the tissue with needle in place for another 4 min.

After the final injection, incision wounds were sealed using Reflex surgical wound 7-mm clips. Mice were allowed to recover in their home cages heated using a recirculating warm water pad and were postoperatively injected subcutaneously with 0.5-ml saline and buprenorphine dosed at 0.05–0.1 mg/kg for at least 5 d after surgery for pain management. Reflex clips were removed after 7 d.

#### *Dorsal hemisection*

Dorsal hemisection surgeries were conducted as described (Geoffroy et al., 2015) by a surgeon blinded to both genotype and viral injection condition on mice four weeks after AAV injection. Mice were anesthetized with i.p. K/X. The spinal cord was exposed at the level of T8 by laminectomy, followed by bilateral transection of the dorsal spinal cord at the depth of 0.7 mm using marked microfeather scalpel and microdissection scissors. Overlying muscles were sutured together, and the wound was stapled shut using Reflex wound closure systems.

Mice recovered on a recirculating warm water pad and were postoperatively injected subcutaneously with saline and buprenorphine. For at least the next 5 d up to the next eight weeks, pain management was achieved using buprenorphine, and infections were treated with Baytril. In mice that failed to recover urinary control, manual bladder expression was conducted twice daily for as many days as necessary to prevent urinary tract infections.

#### *Unilateral pyramidotomy*

Pyramidotomy surgeries were conducted two weeks after AAV injections using previously described methods with slight modifications (Starkey et al., 2005). Mice were anesthetized with i.p. K/X and placed on the stage of a dissection microscope with ventral side facing up. An incision was made to expose the esophagus and neighboring muscles of the neck. Blunt dissection was used to expose the medullary pyramids at the base of the skull. Using a premarked surgical microfeather scalpel, a 0.7-mm-deep incision is made transecting only the animal's left medullary pyramid anterior to the decussation site. Wounds were closed using skin glue (Vetbond, 3M), and mice recovered with heat support and were postoperatively injected with saline and buprenorphine.

#### *Biotinylated dextran amine (BDA) tracing*

Injections of anterograde tracer BDA were conducted two weeks after pyramidotomy surgeries or six weeks after dorsal hemisection. Stock 10% BDA (10,000 MW, Thermo Fisher Scientific) prepared in sterile PBS was injected to the same coordinates using the same injection protocols as described above for AAV injections. Wounds were closed with Reflex clips and mice treated postoperatively with saline and buprenorphine. Mice were killed two weeks later.

#### **Tissue processing**

Mice were administered a lethal dose of Fatal Plus (pentobarbital sodium) and perfused transcardially with freshly made ice-cold 4% paraformaldehyde (PFA) solution; brain and spinal cord were dissected out and postfixed overnight in 4°C PFA solution. Subsequently, tissues were incubated for 72 h at 4°C in 30% sucrose solution for cryoprotection before embedding in Tissue-TEK OCT Compound and freezing over dry ice.

For regeneration studies, brain, medulla, and 8 mm thoracic spinal cord segments centered at the dorsal hemisection injury site, with additional 2-mm segments immediately rostral and caudal, were collected and embedded in OCT compound and frozen on dry ice. Tissues were cut on a cryostat to a thickness of 20  $\mu$ m. The 2-mm rostral/caudal segments were sliced transversely and stained for BDA to assess completeness of injury. Mice would be excluded if caudal transverse sections showed labeled CST axons in the dorsal main tract (most likely because of sparing); however, no subjects in the current study met this exclusion criteria. Medullas were sliced transversely to obtain estimates of total number of CST axons labeled to control for labeling efficiency (see below). Sagittal sections of the 8-mm segment of thoracic spinal cord

were sliced and stained for both GFAP (rat anti-GFAP, 1:200 dilution, Invitrogen) and BDA. Lastly, brains were cut coronally at 20- $\mu$ m thickness and stained for pS6 or processed for BaseScope.

For sprouting studies, brain, medulla, and a 2-mm segment of cervical spinal cord at C5–C7 levels were collected. Cervical spinal cord was sliced in 20- $\mu$ m transverse sections and immunostained for PKC $\gamma$  to assess completeness of injury. Animals that showed bilateral PKC $\gamma$  signal were excluded from the study. Cervical spinal cord sections were further stained for BDA and analyzed for midline crossing axons. As with regeneration studies, medullas and brains were similarly sliced and processed.

#### **Staining**

##### *Immunohistochemical staining*

Cervical spinal cord tissues were stained for PKC $\gamma$  (1:200 dilution rabbit anti-PKC $\gamma$ , Santa Cruz Biotechnology), while brain tissues were stained for pS6 (1:200 rabbit anti-pS6, Cell Signaling). Transverse cervical spinal cord and medullas were generally stained free floating, while coronal brains were stained slide mounted. For slide mounted immunostaining, sections were mounted onto Superfrost Plus slides (Thermo Fisher Scientific) in PBS, and then baked onto the slides for a minimum of 30 min in a 37°C oven. Before the blocking step, mounted tissue was rinsed in PBS on an orbital shaker for 10 min. Tissues were blocked in 5% normal goat serum (NGS; Vector Labs) in PBS with 0.4% Triton X-100 (PBS-Tx) for 1–2 h and incubated overnight at 4°C in primary antibody solution made with 2% NGS in PBS-Tx. The next day, sections were rinsed in PBS-Tx and then incubated in a light-protected box with the appropriate secondary antibodies. For free floating stains, secondaries were conducted at a 1:500 dilution; for slide-mounted immunostaining, secondaries were made at a 1:200 dilution. After secondary incubation, sections were rinsed and optionally incubated for 5 min in a 1:2000 dilution of DAPI (Abcam), before drying completely and coverslipping using Fluoromount-G.

##### *BDA staining*

For thoracic and lumbar transverse sections in regeneration studies, cervical transverse sections in sprouting studies, and all medullas, sections were stained free floating for BDA. Slices were permeabilized in two 30 min wash steps in PBS with 0.1% Tween 20 (PBS-Tw). These slices were then incubated overnight at 4°C in Vectastain ABC Solution made at 1:1000 dilution of parts A and B (Vector Laboratories). The next day, the slices were washed in two 1-h steps in 1 $\times$  PBS, before being mounted onto Superfrost Plus slides. After tissue was sufficiently dried onto the slides, hydrophobic borders were drawn on the edges of the slide using PAP pen. The BDA signal was amplified using the TSA Plus Cy3 system (Akoya Bio, formerly PerkinElmer) for 10 min at room temperature at a 1:200 dilution in PBS. Slices were subsequently rinsed in PBS, and then allowed to dry before placing coverslips using Fluoromount-G.

For regeneration studies, to visualize both the GFAP+ scar border and CST axons, sagittal sections of thoracic spinal cord were stained for GFAP using a 1:200 dilution of monoclonal rat anti-GFAP antibody (Invitrogen) and a 1:500 dilution of Alexa Fluor 647 goat anti-rat antibody (Invitrogen), and subsequently stained for BDA following standard protocols. Sections were incubated with 1:2000 dilution of DAPI before placing coverslips with Fluoromount-G.

##### *BaseScope for RNA in brain tissue*

To confirm DLK and LZK deletion in Cre-injected brain tissue, a custom fluorescent BaseScope Red Assay kit (ACD Biotechne) was used to detect DLK or LZK mRNA. Custom ZZ probes targeting the floxed exon were designed using proprietary technology. Hybridization was performed per vendor specifications. For each experimental or control condition, four coronal brain sections measuring 20  $\mu$ m in thickness from three animals per genotype were selected spanning the region of AAV-Cre injections. These were mounted and baked onto Superfrost Plus (Thermo Fisher Scientific) slides and blocked for endogenous peroxidase activity; subsequently slides underwent antigen retrieval treatment and allowed to dry overnight. The following day, sections underwent protease treatment and probes were hybridized and amplified. Signal was detected



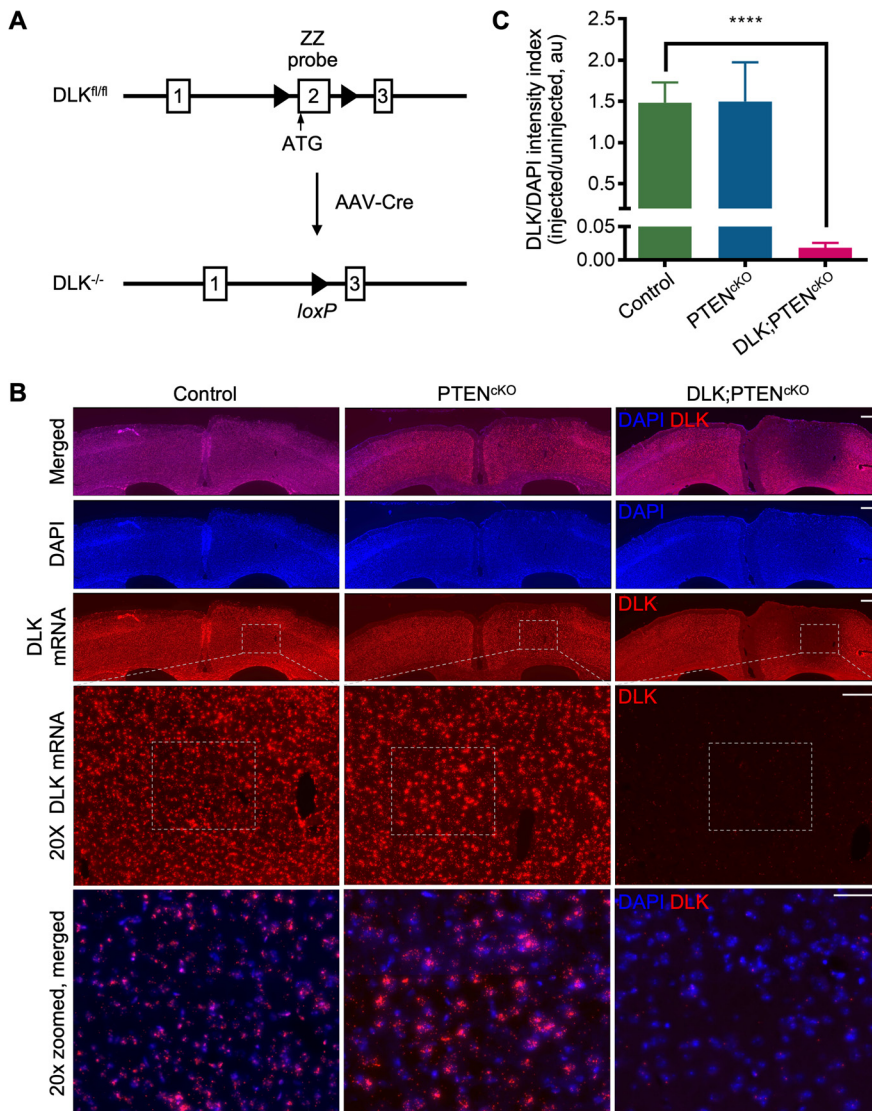


**Figure 1.** Validation of Cre-mediated deletion of DLK using BaseScope in DLK;PTEN<sup>ckO</sup> mice injected with AAV-Cre. **A**, Illustration of DLK<sup>fl/fl</sup> conditional alleles before and after AAV-Cre-mediated deletion of exon 2. The first three exons are depicted as open boxes, while LoxP sites are depicted as black triangles. BaseScope probes were custom designed to recognize the excised sequence in exon 2, depicted as “ZZ.” Allelic elements are not drawn to scale. **B**, Representative images of DLK mRNA signals by BaseScope in control, PTEN<sup>ckO</sup>, and DLK;PTEN<sup>ckO</sup> mice. Scale bar: 300 μm (top 3 rows), 100 μm (20× DLK mRNA in Layer V), 50 μm (20× zoomed, merged, bottom row). **C**, Quantification of DLK mRNA signals relative to DAPI signals measured in AAV-injected hemisphere normalized to uninjected hemisphere. There was a significant reduction of DLK signals in DLK;PTEN<sup>ckO</sup> mice compared with control mice (one-way ANOVA,  $F_{(2,23)} = 22.78$ , \*\*\*\* $p < 0.0001$ ).

with TSA Plus-Cy3 (Akoya Biosciences) and counterstained with DAPI for nuclei; 10× images were taken spanning the entire cerebral cortex, and 20× images were taken within Layer V.

## Quantification

### Rostral axon density index

Methods to quantify rostral axon densities were adapted from previously described (Liu et al., 2010). To determine rostral axon density index, sagittal thoracic spinal cord sections containing the labeled descending CST were stained for BDA and GFAP, and then imaged on an upright Zeiss Axio Imager M1 microscope using a 10× objective. Images were analyzed using ImageJ (NIH). The injury site was identified with GFAP+ scar border, and fifteen 100-μm boxes spanning the dorsal-ventral width of each section were drawn rostral to the injury epicenter, covering a total distance of 1.5 mm. Axon density measures were calculated for each box by measuring the average intensity within each box, and subtracting the average intensity of background signal as measured in a 100-

μm region with no BDA signal caudal to the site of injury. This value was then normalized to the axon density measured at 1.4–1.5 mm rostral to the injury site as described (Liu et al., 2010; Geoffroy et al., 2015). For each animal, five to eight sections containing main CST were analyzed and averaged together. Axon density indices ± SEMs were plotted as a function of distance rostral to the site of injury.

### Caudal regeneration index

Quantification of axon regeneration caudal to injury was adapted from previously described (Lee et al., 2010) on the same set of images taken on 8-mm sagittal sections of the spinal cord. Using an automated macro wherein a blind observer identified the injury site via GFAP staining, 43 boxes each measuring 50 μm (length) × 2000 μm (width) were aligned to the injury site. The number of axons crossing at each 50-μm increment was counted manually in as many sections containing CST labeling (five to eight sections per animal). Counts at each distance were averaged for each animal and normalized against total axon count measured in the medulla to obtain a caudal regeneration index, which was plotted as a function of distance caudal from the injury site (Geoffroy et al., 2015).

### Sprouting index

As described (Lee et al., 2010; Geoffroy et al., 2015), transverse C5–C7 spinal cord sections were sliced and stained for BDA-labeled CST axons. Images were analyzed using FIJI/ImageJ software. A custom FIJI/ImageJ macro was developed to automatically align boxes measuring 50 or 100 μm to a user-indicated midline. The first box measured 50 μm in width, and remaining boxes measured 100 μm extending up until 1100 μm away from the indicated midline. Axon crossover events at each of these distances were manually quantified by a blinded individual. For each animal, five to seven sections are quantified, and counts at every indicated distance were averaged, and then normalized against the medullary total axon count (see below). Axon sprouting index ± SEM is plotted as a function of distance away from the midline into the denervated side.

### Total axon count

Total axon counts are measured to normalize caudal regeneration and sprouting indices. Medullas were stained for BDA, and two to four medulla sections were imaged with 100× oil objective lens and analyzed on ImageJ using the Find Maxima plugin, which calculates a number of local maxima given a specific prominence value. To set a prominence, several different prominence thresholds were tested on one section from five animals and were double checked using previously described manual counting methods (Lee et al., 2010) to set an established prominence value for the remaining animals/sections in the cohort. Separate prominence values were defined for each batch of stained medulla tissue.

### Intensity indices for BaseScope and immunohistochemistry signals in brain tissue

Coronal sections of brains from mice were either stained for pS6 or underwent BaseScope for either DLK or LZK mRNA. For quantification,

three to four animals were analyzed per genotype, and four sections were analyzed from each animal throughout the region of the injected areas. Quantifications were conducted with ImageJ by a genotype-blinded observer. To quantify pS6 staining, a composite index for signal intensity in Layer V neurons (identified with DAPI counterstain) was calculated for each hemisphere. The injected hemisphere was identified either via GFP signal in the control mice, or gross changes in tissue structure secondary to injection (e.g., needle tracks, brain swelling) and/or PTEN deletion where applicable (Gutilla et al., 2016; Gallent and Steward, 2018) in Cre-injected mice;  $300 \times 300\text{-}\mu\text{m}$  boxes were drawn over Layer V neurons in both hemispheres equidistant from the central fissure. Following background subtraction, the Analyze Particles plugin of ImageJ was used to threshold pS6 positive areas. The resultant images were segmented into particles, and these particles' size and average intensity were calculated for both hemispheres. The total area within each box above threshold was multiplied to the average intensity of the signal to provide a composite measure of pS6 signals for each hemisphere, and then the ratio of pS6 signals in the injected versus uninjected hemispheres was obtained as the pS6 intensity index. For DLK/DAPI signal, composite indices were calculated similarly as pS6 first by calculating the ratio of DLK mRNA/DAPI signals from Layer V neurons, and then the value in the injected hemisphere was then normalized to that in the uninjected hemisphere to obtain the DLK/DAPI intensity index. BaseScope data on LZK mRNA was quantified in the same way as for DLK. The following settings were used on the Analyze Particles plugin: pS6 and DLK/LZK size: 6–infinity, circularity  $-0\text{--}1$ ; DAPI size 50–infinity, circularity  $-0\text{--}1$ .

#### Counting DAPI+ cells in brain tissue processed for BaseScope

To measure cell density, DAPI+ nuclei were manually counted in coronal brain sections processed for BaseScope and counterstained with DAPI (described above). For each genotype, three to four animals were used and for each animal three to four sections were analyzed. In ImageJ, a  $150 \times 100\text{-pixel}$  window (translating to  $96.77 \times 64.52\ \mu\text{m}$ ) was drawn over Layer V neurons in the DAPI channel. Within each region, DAPI+ cells were manually counted for both AAV-injected and uninjected hemispheres. To calculate the difference in cell density across genotypes, the number of DAPI+ cells counted in the AAV-injected hemisphere were normalized to DAPI+ cells in the uninjected hemisphere.

#### Experimental design and statistical analysis

Sprouting, regeneration and axon density index data were analyzed following genotype blinding protocols, using two-way repeated measures (RM) ANOVA with Bonferroni *post hoc* test. Intensity analyses for pS6 and BaseScope results were analyzed with one-way ANOVA or Student's *t* test where appropriate, as were total axon counts. For all statistical analyses, GraphPad Prism 6 was used with a  $p < 0.05$  set as the threshold for statistical significance after Bonferroni correction for multiple comparisons. These are denoted in graphs with asterisks. All data are displayed as

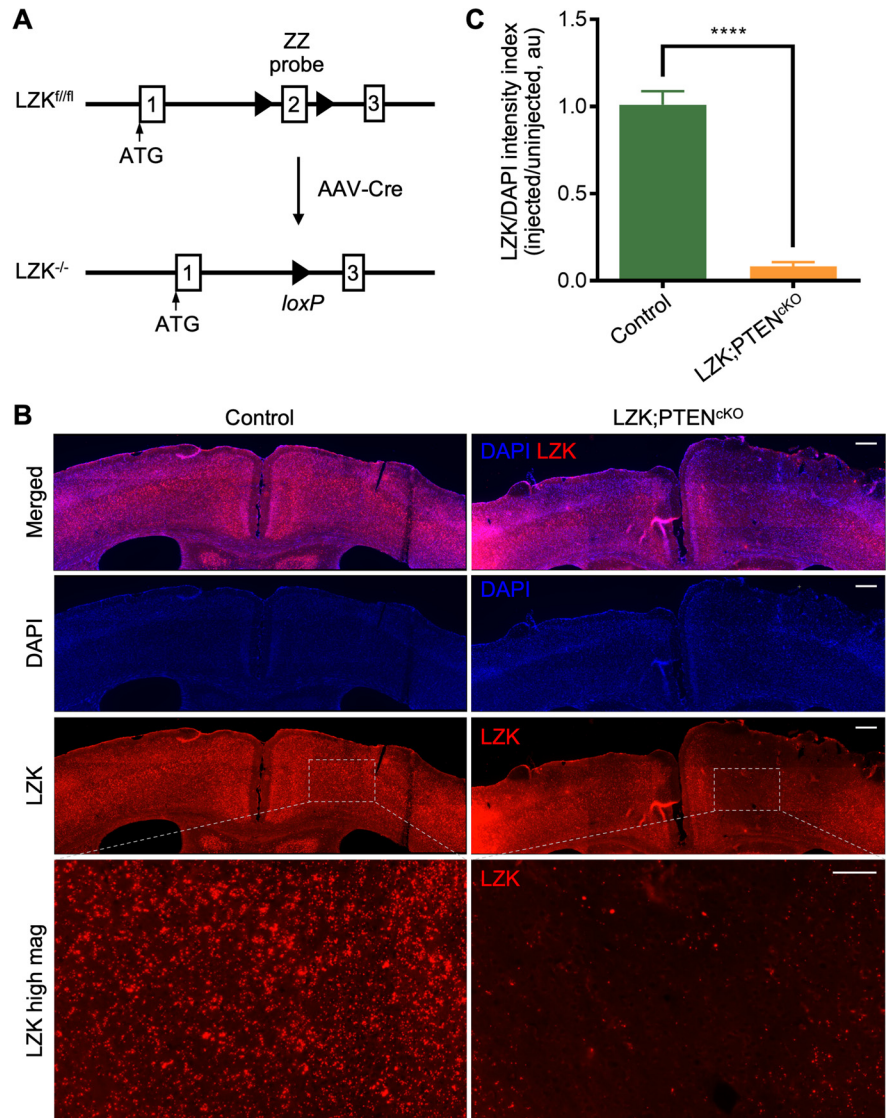


**Figure 2.** Validation of Cre-mediated deletion of LZK using BaseScope in LZK;PTEN<sup>cko</sup> mice. **A**, Illustration of LZK<sup>fl/fl</sup> conditional alleles before and after AAV-Cre-mediated deletion of exon 2. ZZ probes were custom designed to detect exon 2 with BaseScope. Allelic elements are not drawn to scale. **B**, Representative images of LZK mRNAs signals with BaseScope in control and LZK;PTEN<sup>cko</sup> mice. Scale bar: 300  $\mu\text{m}$  (low mag), 100  $\mu\text{m}$  (high mag, bottom panels). **C**, Quantification of LZK mRNA signals relative to DAPI measured in AAV-injected hemisphere normalized to uninjected hemisphere in control and LZK;PTEN<sup>cko</sup> mice (two-tailed unpaired *t* test, \*\*\*\* $p < 0.0001$ ).

means, with error bars denoting  $\pm$ SEM. Specific *n* values for each study are noted in figure legends.

## Results

### Establishing and validating inducible gene KO mice

We hypothesized that neuronal DLK and LZK positively regulate axon regeneration in the mammalian spinal cord. A genetic test would entail conditional gene deletion of DLK and/or LZK followed by an assessment of the regeneration phenotype using a model system such as the CST. Because CST axons normally do not exhibit significant regeneration after spinal cord injury, we used PTEN deletion to attain an elevated baseline level of CST regeneration (Liu et al., 2010) so that a reduction in regeneration could be readily detected. Accordingly, we bred previously validated DLK<sup>fl/fl</sup> and LZK<sup>fl/fl</sup> conditional alleles (Chen et al., 2016, 2018; Li et al., 2021; Figs. 1A, 2A) to PTEN<sup>fl/fl</sup> mice to obtain



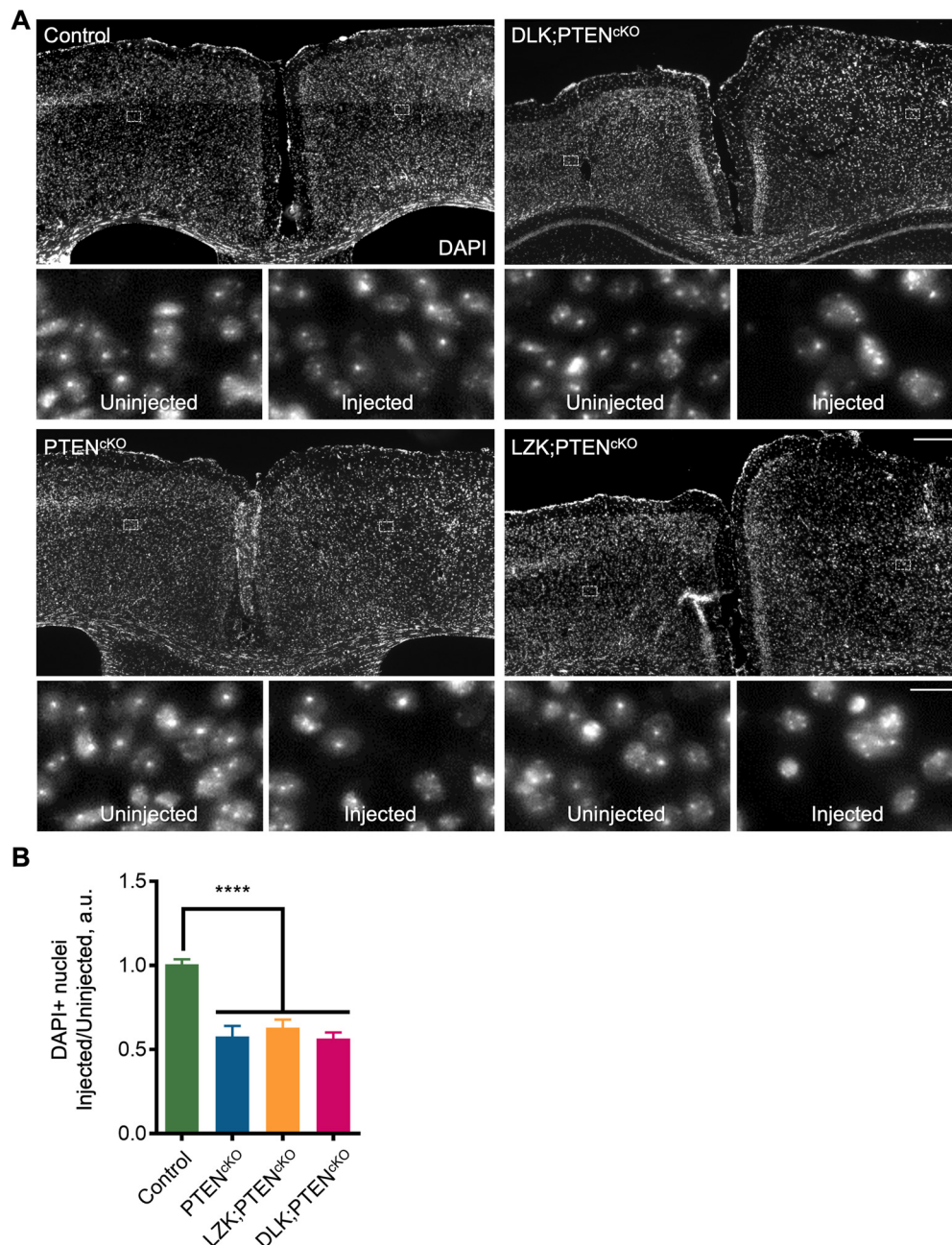


**Figure 3.** Reduced cell density as assessed with DAPI staining in AAV-Cre injected hemisphere of PTEN<sup>cKO</sup>, DLK;PTEN<sup>cKO</sup>, and LZK;PTEN<sup>cKO</sup> mice. **A**, Representative images of DAPI staining across different mouse lines at low and high magnifications. Scale bars: 300  $\mu$ m (low mag), 20  $\mu$ m (high mag). **B**, Quantification of DAPI+ nuclei in the AAV-injected hemisphere normalized to DAPI+ nuclei in the uninjected hemisphere. One-way ANOVA revealed significant differences across genetic conditions ( $F_{(3,44)} = 36.94$ ,  $p < 0.0001$ ). Multiple comparisons with Bonferroni's correction confirmed significant reductions in cell density for the AAV-Cre-injected hemisphere of PTEN<sup>cKO</sup>, LZK;PTEN<sup>cKO</sup>, and DLK;PTEN<sup>cKO</sup> mice (\*\*\*\* $p < 0.0001$  for all genotypes).

various combinations of homozygous double and triple conditional mutants, all in C57BL/6 background. Floxed exon 2 of *DLK* contains the ATG start codon, whereas deleting exon 2 of *LZK* places all downstream exons out of frame. AAV-Cre virus was injected into the sensorimotor cortex of six-week-old mice to induce gene deletion; these mice would be referred to as cKO, designated as DLK<sup>cKO</sup>, LZK<sup>cKO</sup>, PTEN<sup>cKO</sup>, DLK;LZK<sup>cKO</sup>, DLK;PTEN<sup>cKO</sup>, LZK;PTEN<sup>cKO</sup> or DLK;LZK;PTEN<sup>cKO</sup>. Littermates that received AAV-GFP injections served as controls.

To confirm DLK and LZK gene deletion following AAV-Cre injections, we leveraged the newly available custom fluorescent BaseScope assay to detect short RNA targets with high sensitivity and specificity (see Materials and Methods). Unlike regular

RNAScope that requires RNA targets to be >300 nt in size, BaseScope probes (designated ZZ) can detect RNA targets of 50–300 nt, widely adaptable for detecting single exon deletion. Target-specific ZZ probes were custom designed with proprietary technology to bind the floxed exon 2 of the DLK or LZK gene (Figs. 1A, 2A). PTEN<sup>fl/fl</sup>, DLK<sup>fl/fl</sup>;PTEN<sup>fl/fl</sup>, and LZK<sup>fl/fl</sup>;PTEN<sup>fl/fl</sup> mice received AAV-Cre or control AAV-GFP injections in the right sensorimotor cortex, leading to intended gene deletion in cKO mice or GFP expression in control mice, followed by dorsal hemisection spinal cord injury four weeks later.

Control mice exhibited uniform DLK or LZK mRNA puncta bilaterally throughout the cortical layers including Layer V,

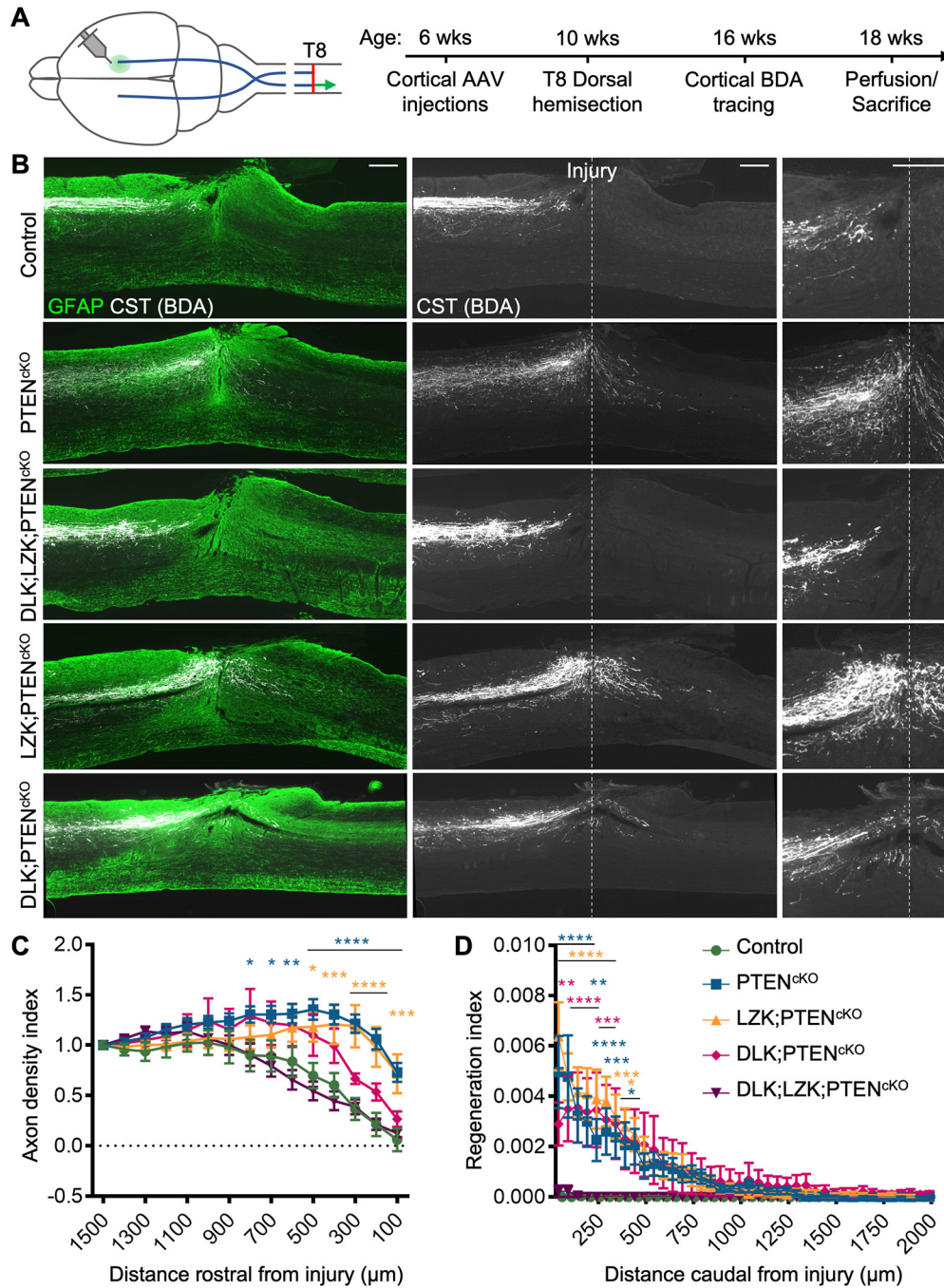


**Figure 4.** Co-deletion of DLK and LZK blocks PTEN deletion-induced CST axon regeneration after dorsal hemisection spinal cord injury. **A**, Experimental paradigm for dorsal hemisection spinal cord injury. AAV vectors can be AAV-Cre or AAV-GFP. **B**, Representative images of BDA tracing of CST axons (white) with GFAP staining (green) to outline the injury site on sagittal spinal cord sections from control, PTEN<sup>CKO</sup>, DLK;LZK;PTEN<sup>CKO</sup>, LZK;PTEN<sup>CKO</sup>, and DLK;PTEN<sup>CKO</sup> mice. Caudal is to the right. Scale bar: 300 μm. **C**, Quantification of axon density indices rostral to injury as one measure of regeneration. Axon density index was calculated as the average axon intensity normalized to axon density at 1.4–1.5 mm rostral to injury (mean ± SEM). Two-way RM ANOVA revealed significant differences across genetic conditions ( $F_{(14,868)} = 34.10, p < 0.0001$ ). Multiple comparisons with Bonferroni correction revealed elevated densities in PTEN<sup>CKO</sup> at 800 μm,  $p = 0.0328$ ; at 700 μm,  $p = 0.0279$ ; at 600 μm,  $p = 0.0059$ ; at 500–100 μm,  $p < 0.0001$ . LZK;PTEN<sup>CKO</sup> showed significantly elevated densities at 500 μm,  $p = 0.0299$ ; at 400 μm,  $p = 0.0022$ ; at 300–200 μm,  $p < 0.0001$ ; at 100 μm,  $p = 0.0006$ . At 300 and 200 μm rostral to injury, DLK;PTEN<sup>CKO</sup> had significantly lower density than PTEN<sup>CKO</sup> ( $p = 0.015$  and  $0.023$ , respectively;  $p = 0.0672$  at 100 μm). **D**, Quantification of axon regeneration caudal to the injury site. Regeneration index was calculated as the ratio of axon numbers at each defined distance caudal to injury normalized to total axon count labeled in medulla. Two-way RM ANOVA revealed statistically significant differences across genetic conditions ( $F_{(4,62)} = 6.073, p = 0.0003$ ). Multiple comparisons with Bonferroni correction revealed significantly elevated regeneration for PTEN<sup>CKO</sup>: at 50–200 and 300 μm,  $p < 0.0001$ ; at 250 μm,  $p = 0.0023$ ; at 350 μm,  $p = 0.0009$ ; at 400 μm,  $p = 0.0141$ ; at 450 μm,  $p = 0.0255$ . LZK;PTEN<sup>CKO</sup> showed significantly elevated regeneration: at 50–350 μm,  $p < 0.0001$ , at 400 μm,  $p = 0.0009$ ; at 450 μm,  $p = 0.0112$ . DLK;PTEN<sup>CKO</sup> showed significantly elevated regeneration: at 50 μm,  $p = 0.0010$ , at 100–250 μm,  $p < 0.0001$ ; at 300 μm,  $p = 0.0003$ ; at 350 μm,  $p = 0.0009$ . Annotations for statistics for 2c and 2d: \* $p < 0.05$ , \*\* $p < 0.01$ , \*\*\* $p < 0.001$ , \*\*\*\* $p < 0.0001$ .  $N = 17$  (control), 16 (PTEN<sup>CKO</sup>), 17 (DLK;LZK;PTEN<sup>CKO</sup>), 9 (LZK;PTEN<sup>CKO</sup>), 8 (DLK;PTEN<sup>CKO</sup>).



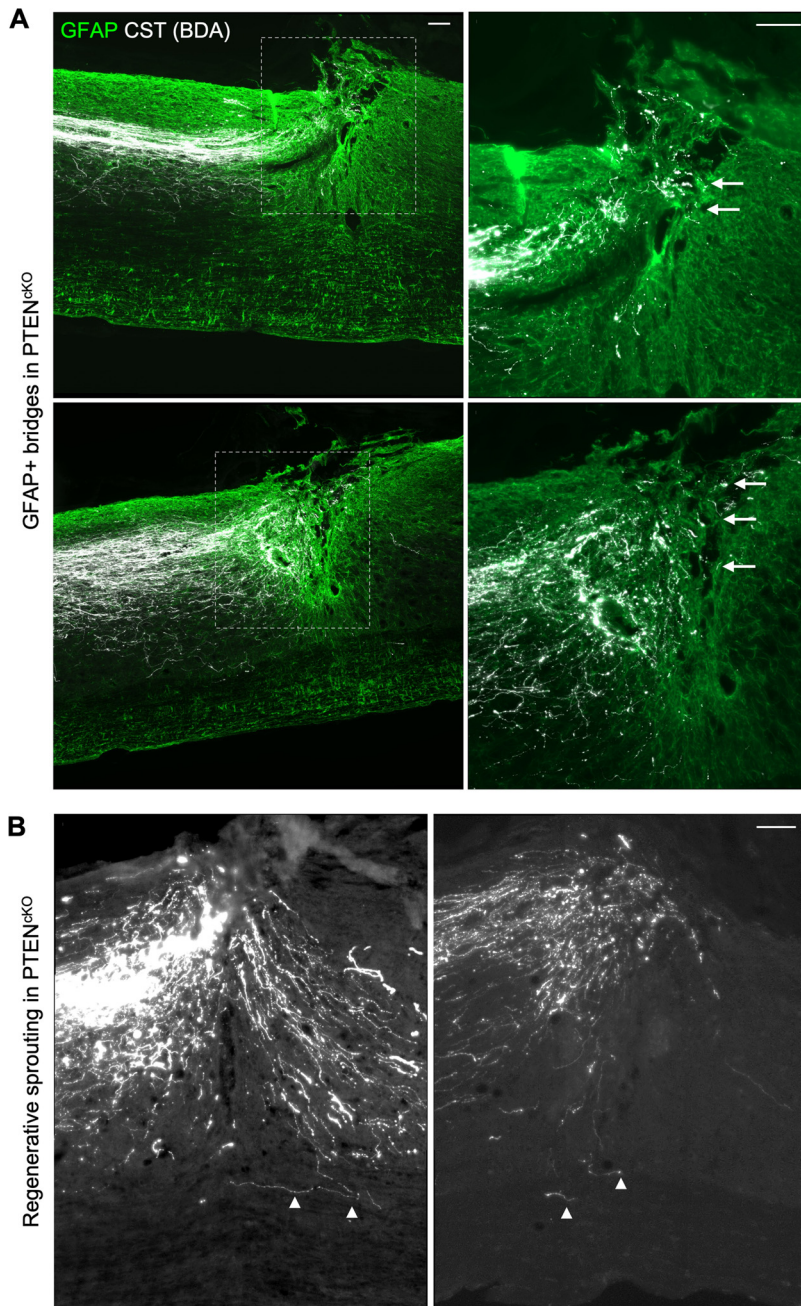


**Figure 5.** Selected features of CST axon regeneration in PTEN-deleted mice. **A**, Representative images of CST axons (white arrows) regenerating through GFAP+ bridges at the injury site in PTEN<sup>ckO</sup> mice. Dotted boxes in left panels are presented at higher magnification in right panels. **B**, Regenerative sprouting of CST axons (white triangles) around the ventral edge of the dorsal hemisection injury in PTEN<sup>ckO</sup> mice. Scale bar: 100  $\mu$ m (**A**, left panels), 100  $\mu$ m (**A**, right panels), 100  $\mu$ m (**B**).

consistent with no genetic perturbation following AAV-GFP injections (Figs. 1B, 2B). Likely reflecting the known cellular hypertrophy caused by PTEN deletion (Liu et al., 2010; Gutilla et al., 2016; Gallent and Steward, 2018), DLK mRNA signals in the AAV-Cre-injected hemisphere of PTEN<sup>ckO</sup> mice appeared more intense and occupied a larger area per cell (Fig. 1B). This cellular hypertrophy was accompanied by a  $\sim$ 40% reduction in cell density as compared with the uninjected hemisphere in PTEN<sup>ckO</sup>, DLK;PTEN<sup>ckO</sup>, and LZK;PTEN<sup>ckO</sup> mice as assessed with DAPI nuclear staining (Fig. 3A,B). This reduced cell density following PTEN deletion may be because of (1) increased cell body size; (2) increased representation of neuropil versus cell bodies (Gutilla et

al., 2016; Gallent and Steward, 2018); and (3) possible atrophy of neighboring cells resulting from PTEN deletion-induced hypertrophy.

Despite the cellular hypertrophy and the accompanying reduction in cell density, PTEN<sup>ckO</sup> mice exhibited a similar ratio of DLK/DAPI signal intensities in the AAV-injected hemisphere as normalized against the noninjected hemisphere (a composite DLK/DAPI intensity index, see Materials and Methods) as control mice (Fig. 1B,C), indicating that PTEN deletion does not interfere with DLK gene expression. In contrast, DLK;PTEN<sup>ckO</sup> mice showed a  $\sim$ 98.7% reduction in DLK mRNA signals within the injected hemisphere using the same measure while exhibiting similarly loosely packed DAPI+ nuclei as PTEN<sup>ckO</sup> mice (Fig. 1B,C). These reductions were consistent across multiple mice per genotype and throughout the A-P axis of the injected area. Likewise, LZK;PTEN<sup>ckO</sup> mice showed a  $\sim$ 92.5% reduction of LZK mRNA signals within the injected hemisphere (Fig. 2B,C). Thus, cortical AAV-Cre injections induced highly efficient DLK and LZK gene deletion in DLK;PTEN<sup>ckO</sup> and LZK;PTEN<sup>ckO</sup> mice, respectively, apparently without affecting the cellular hypertrophy caused by PTEN deletion.

#### DLK and LZK co-deletion blocks PTEN deletion-induced corticospinal axon regeneration

Previous work has shown that within the first seven to 10 d after injury, CST axons undergo axonal dieback, characterized by the formation of dystrophic endbulbs (Liu et al., 2010). While both control and PTEN cKO mice are known to exhibit similar levels of axonal dieback, only PTEN-deleted axons are able to overcome this initial dieback and regenerate toward the lesion, with a small percent of axons regenerating beyond (i.e., through or around) the injury site (Liu et al., 2010). By eight weeks after injury, regenerating axons can be observed both immediately above and below the lesion in PTEN-deleted mice, with the presence of axons caudal to injury generally considered a more definitive indicator of regeneration. If DLK and/or LZK are required for axon regeneration, conditional DLK and/or LZK gene deletion would be expected to substantially reduce CST regeneration normally seen in PTEN<sup>ckO</sup> mice. We therefore compared CST regeneration phenotype among five groups of mice: control, PTEN<sup>ckO</sup>, DLK;LZK;PTEN<sup>ckO</sup>, LZK;PTEN<sup>ckO</sup>, and DLK;PTEN<sup>ckO</sup>. Control mice were littermates with the various cKO alleles that received AAV-GFP injections; these control mice exhibited similar phenotypes and were not distinguished further. Young adult mice underwent cortical AAV injections, followed by T8 dorsal hemisection spinal cord injury four weeks later (Fig. 4A). CST axons were traced with anterograde tracer biotinylated dextran amine (BDA) six weeks after injury, and killed two

weeks later for tissue processing as described (Liu et al., 2010; Geoffroy et al., 2015).

The majority of control mice exhibited dense BDA labeling in the main CST around 1 mm rostral to the lesion. Closer to the injury site, this dense BDA labeling tapered off, and individual axons terminated in retraction bulbs several hundred micrometers rostral to the edge of the GFAP+ scar border (Fig. 4B). Caudal to injury rarely were any labeled CST axons detected in control mice.  $PTEN^{cKO}$  mice also had dense CST labeling rostral to injury but exhibited a much less noticeable drop approaching the injury site, with the bulk of labeled axons appearing to reach the edge of the GFAP+ scar border, often bending dorsally likely because of the mechanics of the dorsal hemisection injury (Fig. 4B). As expected,  $PTEN^{cKO}$  mice typically extended regenerating axons beyond the site of injury. The vast majority of the regenerating axons grew across the dorsal aspect of the lesion, and they appeared to traverse the injury site primarily through GFAP+ bridges (Figs. 4B, 5A, white arrows). In some rare cases labeled axons could be seen growing in the ventral cord and extending beyond the ventral edge of the lesion caudally, which could be offshoots of axonal branches in the gray matter into spared ventral white matter (Fig. 5B, white triangles), a phenomenon referred to as regenerative sprouting (Steward and Willenberg, 2017). Strikingly,  $DLK;LZK;PTEN^{cKO}$  mice exhibited a similar phenotype as the control mice,  $LZK;PTEN^{cKO}$  mice exhibited a similar phenotype as the  $PTEN^{cKO}$  mice, whereas  $DLK;PTEN^{cKO}$  mice exhibited axon regeneration but with a phenotype that was somewhat between control and  $PTEN^{cKO}$  mice (Figs. 4B, 6).

To quantify CST axon phenotype, rostral axon density indices were calculated as axon densities at specified intervals rostral to injury normalized against that at 1.4–1.5 mm rostral to injury; caudal regeneration indices were calculated as axon numbers at specified intervals caudal to injury normalized against the total labeled CST axon counts in the medulla (Fig. 7A; for details, see Materials and Methods), similarly as described (Liu et al., 2010; Geoffroy et al., 2015). One-way ANOVA revealed no significant differences in the total number of labeled axons at the level of the medullas (Fig. 7C,D). Two-way RM ANOVA revealed significant differences across genotypes for both rostral and caudal measures of regeneration (rostral axon densities:  $F_{(14,868)} = 34.10$ ,  $p < 0.0001$ ; caudal regeneration:  $F_{(4,62)} = 6.073$ ,  $p = 0.0003$ ). Multiple comparisons with Bonferroni correction revealed genotype-dependent differences at specified intervals rostral and caudal to injury (Fig. 4C,D).

As expected,  $PTEN^{cKO}$  mice exhibited significantly higher rostral axon densities (100–800  $\mu\text{m}$  rostral to injury) and caudal

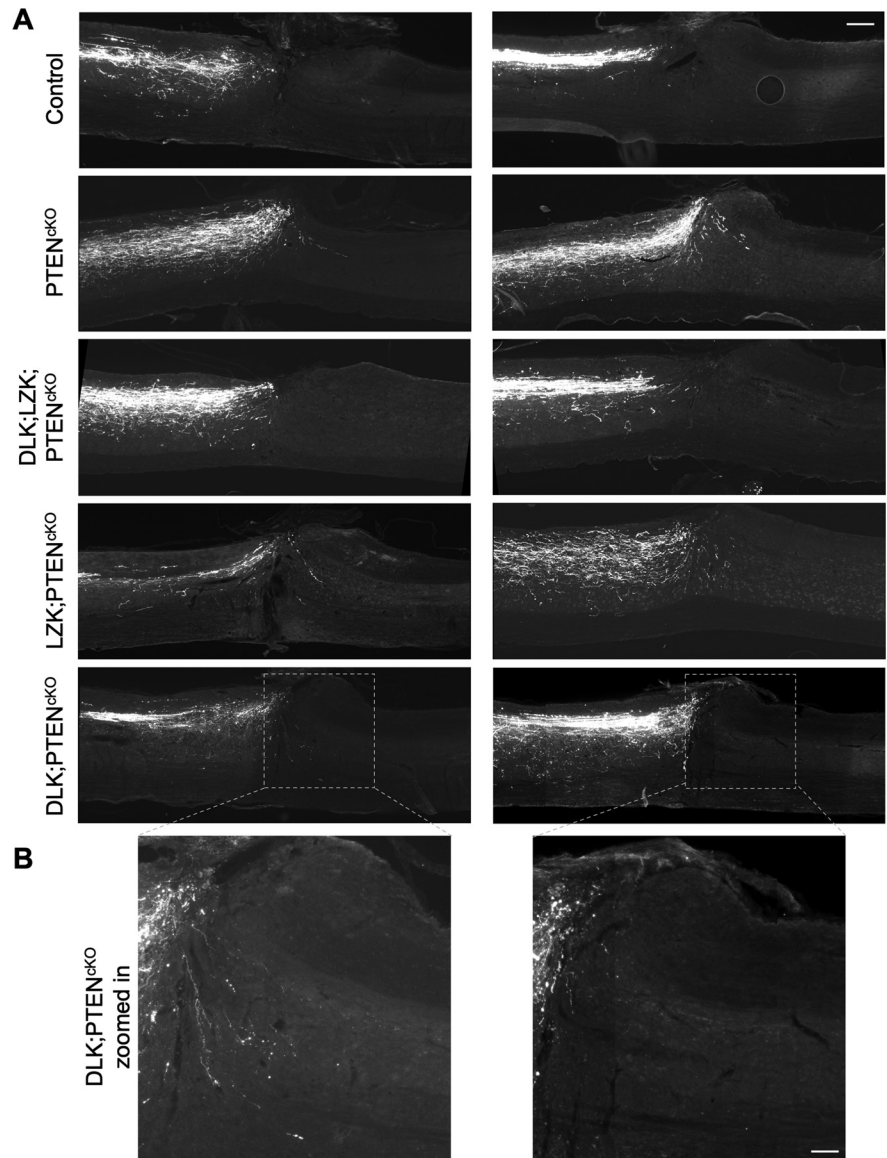


**Figure 6.** Additional examples of BDA tracing of CST axons after dorsal hemisection injury across genotypes. **A**, Representative images from two additional mice per genotype demonstrating the kind of CST regeneration (or lack thereof) observed in different genotypes. **B**, Zoomed in caudal regenerating axons in two different  $DLK;PTEN^{cKO}$  mice demonstrating a more robust regenerator (left) and a less robust regenerator (right).

regeneration (up to 450  $\mu\text{m}$  beyond injury) as compared with control mice (Fig. 4C,D). Rostral to injury,  $DLK;LZK;PTEN^{cKO}$  mice showed axon densities at levels comparable to control mice and substantially lower than  $PTEN^{cKO}$  as the main CST approached the injury site; caudal to injury,  $DLK;LZK;PTEN^{cKO}$  mice exhibited no or little regeneration just as the control mice. In contrast,  $LZK;PTEN^{cKO}$  mice had rostral axon densities similar to  $PTEN^{cKO}$  mice and significantly higher than control mice (100–500  $\mu\text{m}$  rostral to injury); caudal to injury,  $LZK;PTEN^{cKO}$  mice exhibited robust regeneration (up to 450  $\mu\text{m}$  beyond injury), with the majority of individual  $LZK;PTEN^{cKO}$  mice phenotypically indistinguishable from  $PTEN^{cKO}$  mice (Figs. 4B–D, 6A). Compared with  $PTEN^{cKO}$  mice,  $DLK;PTEN^{cKO}$  mice exhibited reduced rostral axon densities (significant at 200 and 300  $\mu\text{m}$  rostral to injury) but remained modestly elevated compared with control mice although that difference did not reach statistical significance. Caudal to injury,  $DLK;PTEN^{cKO}$  mice exhibited significantly elevated CST regeneration as compared



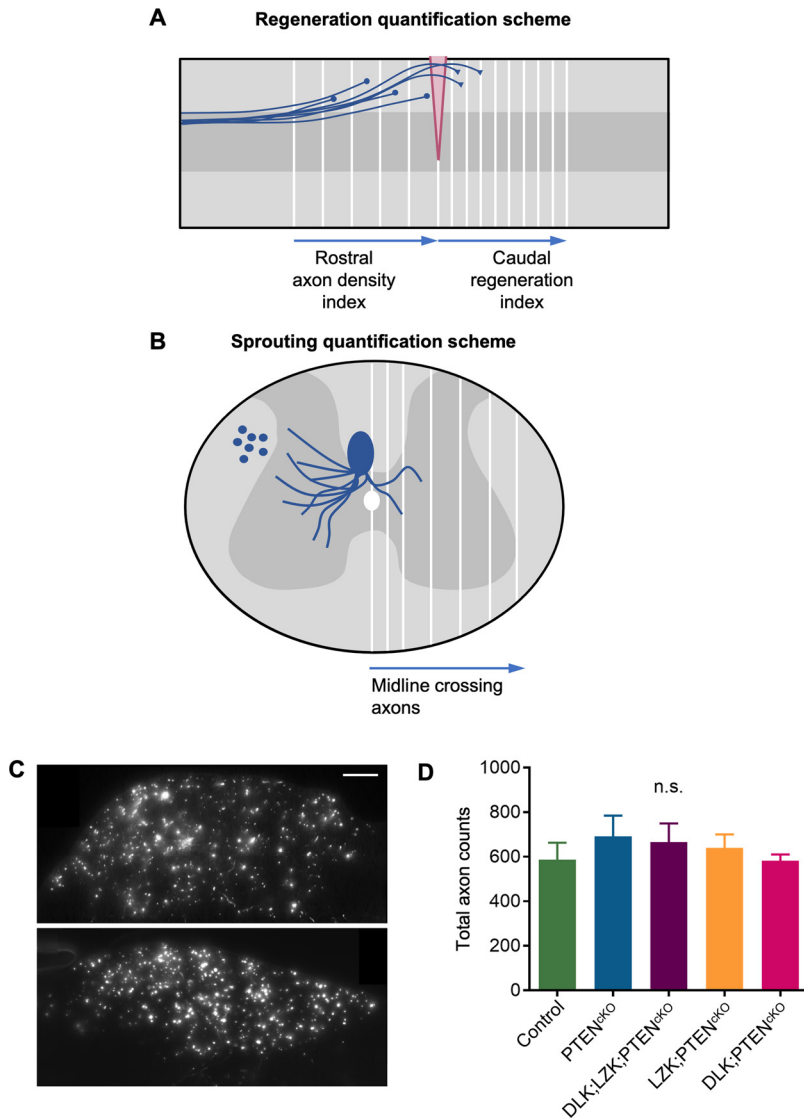


**Figure 7.** Quantification schematics for regeneration, sprouting, and total axon counts. **A**, Illustration of a sagittal section of spinal cord containing the injury site (labeled in pink) with regenerating CST axons. CST axons are depicted in blue, with axons that failed to regenerate rostral to the site of injury terminating in dystrophic endbulbs (circles), and axons regenerating beyond the injury site ending in growth cones (reverse triangles). Rostral to injury, axon intensity indices were calculated as axon intensities in 100- $\mu$ m regions (rectangles bordered by adjacent white lines) normalized to axon intensity measured at 1.4–1.5 mm rostral to the injury site. Caudal to injury, regeneration indices were calculated as axon numbers counted manually at 50- $\mu$ m intervals caudal to the injury epicenter (white lines) and then normalized to total axon counts measured in the medulla. **B**, Illustration of C5–C7 transverse spinal cord showing CST axons sprouting across the midline into the contralateral denervated gray matter. Sprouting CST axons in the contralateral gray matter were manually counted at the first two 50 intervals, and subsequently 100- $\mu$ m intervals (white lines) and then normalized to total axon counts measured in the medulla. **C**, Representative images of labeled CST axons in the medulla taken with 100 $\times$  oil objective lens. Total axon counts in the medulla were used to normalize caudal regeneration indices in the dorsal hemisection spinal cord injury model and sprouting indices in the unilateral pyramidotomy model. Scale bar: 50  $\mu$ m. **D**, Quantification of total labeled CST axon counts in the medulla from the regeneration model with dorsal hemisection spinal cord injury. One-way ANOVA revealed no significant differences across groups. n.s., not significant.

with control mice (up to 350  $\mu$ m beyond injury), but regeneration appeared to be more modest than PTEN<sup>ckO</sup> or LZK; PTEN<sup>ckO</sup> mice, with half of the regenerating subjects showing only one or two regenerating axons per slice while the remainder on par with PTEN<sup>ckO</sup> mice (Figs. 4B–D, 6).

Overall, further deleting DLK or LZK did not significantly impact PTEN deletion-induced CST axon regeneration caudal to injury. While the bulk of labeled regenerating axons quantified

across these genotypes terminated around 200–400  $\mu$ m caudal to injury, in a subset of mice a small fraction of axons was consistently detected beyond this distance and often even past 1 mm caudal to injury (Fig. 4B,D). Multiple comparisons with Bonferroni correction indicated that both PTEN<sup>ckO</sup> and LZK; PTEN<sup>ckO</sup> mice had significantly more regeneration than controls up to 450  $\mu$ m caudal to injury, while DLK;PTEN<sup>ckO</sup> mice had significantly more regeneration than controls up to 350  $\mu$ m caudal to injury (Fig. 4D). There was a statistically significant difference in regeneration indices between DLK;PTEN<sup>ckO</sup> and LZK; PTEN<sup>ckO</sup> mice at 50  $\mu$ m caudal to injury ( $p = 0.0002$ , with DLK;PTEN<sup>ckO</sup> mice showing a lower number), which may have resulted from the overall reduced axonal densities rostral to injury in DLK;PTEN<sup>ckO</sup> mice. In total, none of the 17 (0%) control mice and only one of 17 (~6%) DLK;LZK;PTEN<sup>ckO</sup> mice exhibited any caudally regenerating axons, while 14 out of 16 (~88%) PTEN<sup>ckO</sup> mice, 8 out of 9 (~89%) LZK;PTEN<sup>ckO</sup> mice, and 6 out of 8 (~75%) DLK;PTEN<sup>ckO</sup> mice exhibited regeneration. The majority of regenerated axons appeared to transverse the dorsal aspect of the lesion (Figs. 4B, 6), often through the GFAP+ bridges as described above.

Collectively, these data demonstrate that DLK and LZK together are required for PTEN deletion-induced CST regeneration. DLK appears to have a somewhat more prominent role, whereas LZK is dispensable on its own and can only partially functionally compensate for the loss of DLK.

#### DLK and LZK co-deletion blocks PTEN deletion-induced corticospinal axon sprouting

Axonal sprouting from uninjured neurons occurs more readily than regeneration from injured neurons after CNS injury. To determine whether DLK and LZK also regulate this more widespread form of axonal repair in the CNS, we assessed the sprouting of uninjured CST axons in the same set of genetically modified mice described above, starting with a comparison between PTEN<sup>ckO</sup> and DLK;LZK; PTEN<sup>ckO</sup> mice. As the DLK pathway is known to mediate injury signaling (e.g., retrograde transport of injury signaling molecules such as pSTAT3) in injured neurons in the PNS (Shin et al., 2012; Asghari Adib et al., 2018), a priori we did not anticipate that such DLK-mediated injury signaling would also function in uninjured neurons that undergo axonal sprouting. To do this, we applied the unilateral pyramidotomy model (Lee et al., 2010; Liu et al., 2010; Geoffroy et al., 2015), where the left pyramidal tract above the medullary decussation is lesioned, and CST sprouting from the uninjured side (i.e., left side, as the CST crosses the midline at the pyramidal decussation) into the denervated side (right) is characterized with BDA tracing on transverse cervical



spinal cord sections (Fig. 8A). To quantify CST sprouting across the midline, BDA labeled axons were counted at specified intervals across the gray matter of the contralateral, denervated side of the spinal cord, and then normalized to total axon counts in the medulla (Geoffroy et al., 2015; Fig. 7B,C). Just as the regeneration study described above, the elevated levels of CST sprouting with PTEN deletion (Liu et al., 2010; referred to as “induced sprouting” below) would make any moderate reduction in axon sprouting readily detectable.

As compared with control mice, PTEN<sup>CKO</sup> mice expectedly exhibited significantly elevated levels of CST axon sprouting after pyramidotomy, where midline-crossing axons fanned out across the denervated, contralateral gray matter of the cervical spinal cord, often reaching both the dorsal and ventral horns (Fig. 8B,C). The majority of these sprouting axons reached ~300–400 μm from the midline, but a handful extended as far as ~700–800 μm. In contrast, DLK;LZK;PTEN<sup>CKO</sup> mice exhibited lower levels of sprouting that were statistically indistinguishable from control mice. There were no significant differences in the total number of axons labeled in the medulla (Fig. 8D). These results indicate that, just as for regeneration, DLK and LZK together are required for PTEN deletion-induced CST sprouting.

To assess the individual contribution of DLK and LZK in mediating PTEN deletion-induced CST sprouting, we compared CST sprouting in DLK;PTEN<sup>CKO</sup> and LZK;PTEN<sup>CKO</sup> mice relative to PTEN<sup>CKO</sup> and control mice (Fig. 9). PTEN<sup>CKO</sup>, LZK;PTEN<sup>CKO</sup>, and DLK;PTEN<sup>CKO</sup> mice exhibited comparable levels of CST sprouting, all significantly elevated compared with control mice at distances up to ~500 μm past the midline into the contralateral, denervated gray matter (Fig. 9A–C). Two-way RM ANOVA revealed significant differences across genetic conditions for both LZK;PTEN<sup>CKO</sup> ( $F_{(2,28)} = 9.729$ ,  $p < 0.001$ ) and DLK;PTEN<sup>CKO</sup> ( $F_{(2,32)} = 5.290$ ,  $p < 0.05$ ) compared with controls, respectively. One-way ANOVA of total axons labeled in the medulla revealed no significant differences in BDA tracing efficiency among the genetic conditions examined (Fig. 9D,E).

Taken together, these findings largely parallel the results observed in CST regeneration in that DLK and LZK together are required for PTEN deletion-induced sprouting. However, unlike in regeneration where DLK deletion appears to partially reduce regeneration, deletion of each kinase alone has no noticeable effects on PTEN deletion-induced CST sprouting.

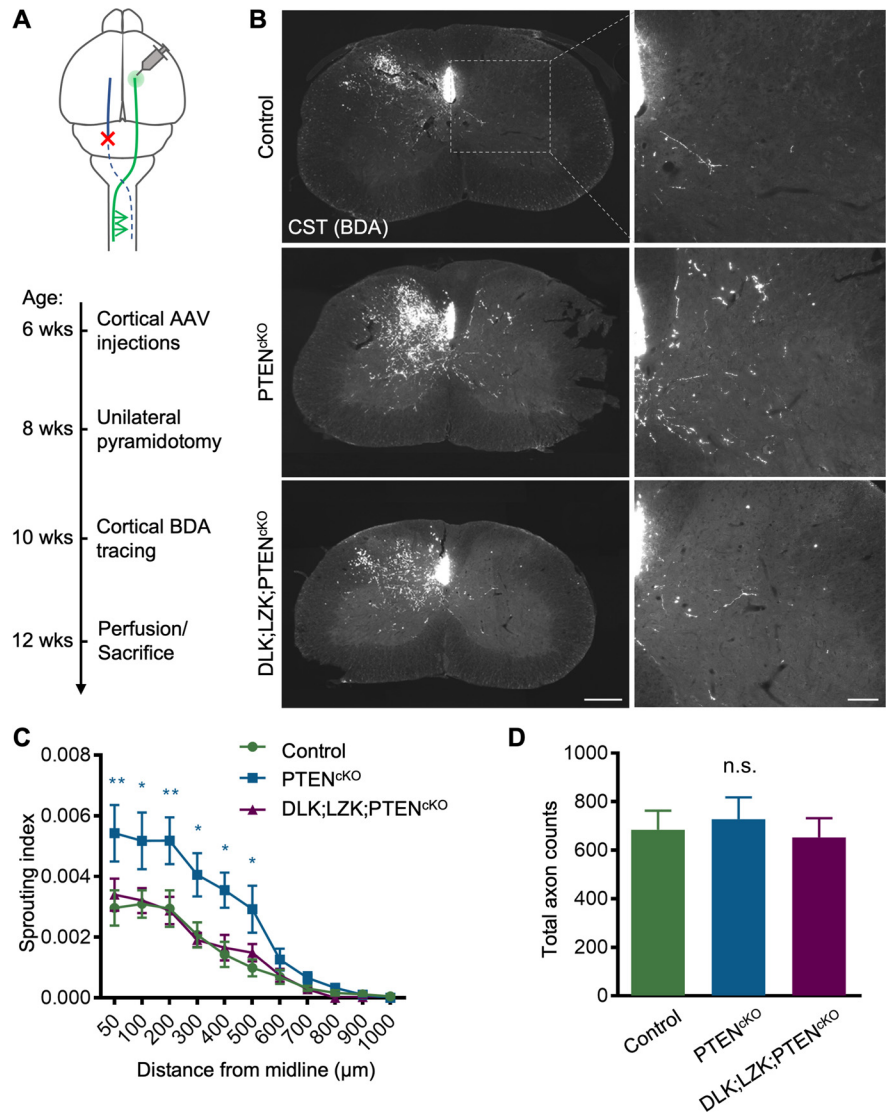


**Figure 8.** Co-deletion of DLK and LZK blocks PTEN deletion-induced CST axon sprouting after unilateral pyramidotomy. **A**, Experimental paradigm for unilateral pyramidotomy. **B**, Representative images of BDA tracing of CST axons (white) on transverse cervical spinal cord sections from control, PTEN<sup>CKO</sup>, and DLK;LZK;PTEN<sup>CKO</sup> mice. Scale bar: 300 μm (left panels), 100 μm (right panels). **C**, Quantification of sprouting. Sprouting index was calculated as the ratio of the average number of axons counted at each distance past midline into the denervated gray matter normalized to the total labeled CST axon count in the medulla (mean ± SEM). Two-way RM ANOVA revealed significant differences across genetic conditions ( $F_{(2,34)} = 5.669$ ,  $p = 0.0075$ ). Multiple comparisons with Bonferroni *post hoc* test revealed elevated sprouting in PTEN<sup>CKO</sup> at 50 μm,  $p = 0.0012$ ; at 100 μm,  $p = 0.0128$ ; at 200 μm,  $p = 0.0052$ ; at 300 μm,  $p = 0.0255$ ; at 400 μm,  $p = 0.0111$ ; at 500 μm,  $p = 0.0322$ . \* $p < 0.05$ , \*\* $p < 0.01$ . **D**, Quantification of total axon counts in medullas; One-way ANOVA, n.s. (not significant).  $N = 13$  (control), 11 (PTEN<sup>CKO</sup>), 13 (DLK;LZK;PTEN<sup>CKO</sup>).

### DLK and LZK co-deletion, but not single gene deletion, suppresses spontaneous CST sprouting

The results above indicate that DLK and LZK together are required for PTEN deletion-induced CST sprouting. To investigate whether DLK and LZK have a more general role in CST sprouting, we asked whether DLK and/or LZK deletion impairs spontaneous sprouting in otherwise wild-type mice by comparing the sprouting phenotype of control, DLK<sup>CKO</sup>, LZK<sup>CKO</sup>, and DLK;LZK<sup>CKO</sup> mice (without the involvement of PTEN<sup>CKO</sup>). Following the same experimental paradigm described for induced sprouting above, we observed no significant differences in CST sprouting among control, DLK<sup>CKO</sup> and LZK<sup>CKO</sup> mice (Fig. 10A,B). Across these three genotypes, low amounts of sprouting were observed throughout the C5–C7 sections

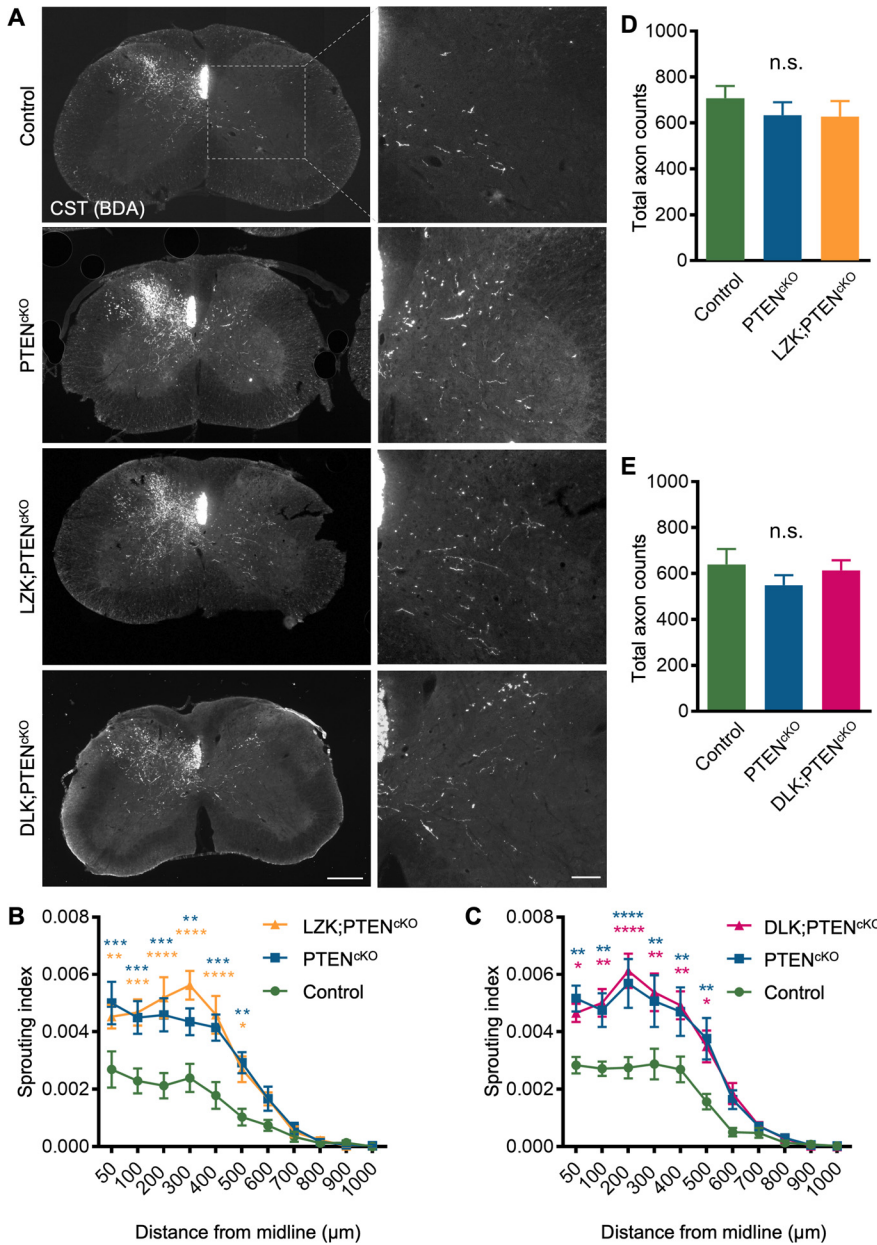


**Figure 9.** Deletion of either DLK or LZK alone does not diminish PTEN deletion-induced CST axon sprouting after unilateral pyramidotomy. **A**, Representative images of BDA tracing of CST axons (white) on transverse cervical spinal cord sections from control, PTEN<sup>ckO</sup>, LZK;PTEN<sup>ckO</sup>, and DLK;PTEN<sup>ckO</sup> mice. Scale bar: 300 μm (left panels), 100 μm (right panels). **B**, Quantification of CST sprouting for LZK;PTEN<sup>ckO</sup> mice in comparison to control and PTEN<sup>ckO</sup> mice. *N* = 9 (control), 10 (PTEN<sup>ckO</sup>), 12 (LZK;PTEN<sup>ckO</sup>). Two-way RM ANOVA revealed significant differences across genetic conditions ( $F_{(2,28)} = 9.729$ ,  $p = 0.0006$ ). Multiple comparisons with Bonferroni correction revealed elevated sprouting for PTEN<sup>ckO</sup>: at 50 μm,  $p = 0.0004$ ; at 100 μm,  $p = 0.0008$ ; at 200 μm,  $p = 0.0001$ ; at 300 μm,  $p = 0.0036$ ; at 400 μm,  $p = 0.0003$ ; at 500 μm,  $p = 0.0003$ . Elevated sprouting for LZK;PTEN<sup>ckO</sup> was observed: at 50 μm,  $p = 0.0045$ ; at 100 μm,  $p = 0.0001$ ; at 200 μm,  $p < 0.0001$ ; at 300 μm,  $p < 0.0001$ ; at 400 μm,  $p < 0.0001$ ; at 500 μm,  $p = 0.0120$ . **C**, Quantification of CST sprouting for DLK;PTEN<sup>ckO</sup> mice in comparison to control and PTEN<sup>ckO</sup> mice. *N* = 10 (control), 14 (PTEN<sup>ckO</sup>), 11 (DLK;PTEN<sup>ckO</sup>). Two-way RM ANOVA revealed significant differences across genetic conditions ( $F_{(2,32)} = 5.290$ ,  $p = 0.0104$ ). Multiple comparisons with Bonferroni correction revealed elevated sprouting for PTEN<sup>ckO</sup>: at 50 μm,  $p = 0.0016$ ; at 100 μm,  $p = 0.0069$ ; at 200 μm,  $p < 0.0001$ ; at 300 μm,  $p = 0.0033$ ; at 400 μm,  $p = 0.0080$ ; at 500 μm,  $p = 0.0032$ . Elevated sprouting for DLK;PTEN<sup>ckO</sup> was observed: at 50 μm,  $p = 0.0297$ ; at 100 μm,  $p = 0.0036$ ; at 200 μm,  $p < 0.0001$ ; at 300 μm,  $p = 0.0013$ ; at 400 μm,  $p = 0.0048$ ; at 500 μm,  $p = 0.0193$ . \* $p < 0.05$ , \*\* $p < 0.01$ , \*\*\* $p < 0.001$ , \*\*\*\* $p < 0.0001$ . **D, E**, Total axon counts in the medulla for the LZK;PTEN<sup>ckO</sup> and DLK;PTEN<sup>ckO</sup> sprouting cohorts, respectively. One-way ANOVA, n.s. for both.

collected. Despite this low baseline level of sprouting, we observed a further reduction of CST sprouting in DLK;LZK<sup>ckO</sup> mice compared with control mice (Fig. 10A,B). Two-way RM ANOVA revealed significant differences across genetic

conditions ( $F_{(3,40)} = 3.708$ ,  $p = 0.0190$ ). Multiple comparisons with Bonferroni correction revealed that DLK;LZK<sup>ckO</sup> mice had significantly reduced sprouting compared with control mice at distances of 50–400 μm from the midline into the denervated gray matter. A caveat to this study was the uneven labeling efficiencies across genetic conditions; one-way ANOVA on total axon counts revealed significantly higher numbers of labeled CST axons in DLK<sup>ckO</sup> and DLK;LZK<sup>ckO</sup> mice compared with control conditions (Fig. 10C). Because this variability was already accounted for by normalizing the data to total labeled axon counts in the medulla (Lee et al., 2010; Liu et al., 2010; Geoffroy et al., 2015), and it did not correlate with the sprouting phenotypes, it likely did not affect the overall sprouting outcome. Thus, in addition to being required for PTEN deletion-induced CST sprouting, DLK and LZK together are important for spontaneous CST sprouting in otherwise wild-type mice.

**DLK and LZK co-deletion does not interfere with mTOR signaling in PTEN-deleted mice**

There are two plausible ways DLK/LZK-dependent injury signaling and PTEN/mTOR-dependent regenerative competence can interact in regulating the regenerative outcome after CNS injury. In one scenario, injury signaling may be required to establish the regenerative competence. Alternatively, injury signaling may work in parallel to the establishment of regenerative competence such that only when both conditions are met (i.e., coincident), a positive regenerative outcome ensues. To distinguish between these two possibilities, we examined levels of phosphorylated ribosomal protein S6 (pS6), a surrogate marker of mTOR activity, following DLK and LZK deletion.

Coronal brain sections of mice that underwent dorsal hemisection or pyramidotomy injury were stained for pS6. In both surgical models, all mice with PTEN deletion in one hemisphere exhibited profound elevations of pS6 signals spanning across multiple cortical layers including Layer V (Figs. 11A, B, Figs. 12). This occurred regardless of whether these PTEN<sup>ckO</sup> mice were also LZK<sup>ckO</sup> and/or DLK<sup>ckO</sup>, such that LZK;PTEN<sup>ckO</sup>, DLK;PTEN<sup>ckO</sup>, and DLK;LZK;PTEN<sup>ckO</sup> mice had significantly (~4-fold) higher pS6 levels in the injected hemisphere as compared with control mice but did not differ significantly from PTEN<sup>ckO</sup> mice.

As expected, in the dorsal hemisection model, AAV-GFP injected control mice did not exhibit a difference in pS6 levels



between the injected hemisphere and the uninjected hemisphere (Fig. 11B), indicating that cortical injections alone did not affect pS6 levels. In the pyramidotomy model, control mice showed a modest (~33%) reduction in pS6 levels in the axotomized but uninjected hemisphere relative to the AAV-GFP injected but uninjured hemisphere (Fig. 12B). Previous studies indicate that axonal injury reduces pS6 levels in corticospinal neurons (Liu et al., 2010). This ~33% reduction of pS6 levels likely represents an underestimation in the reduction of pS6 in axotomized corticospinal neurons because corticospinal neurons are only a subset of the neuronal population sampled for pS6 quantification in the current study. Nonetheless, PTEN deletion, regardless of concurrent DLK and/or LZK deletion, clearly elevated pS6 levels.

Taken together, these data indicate that in either injury model, genetically deleting both DLK and LZK, which mediate injury signaling, does not interfere with PTEN/mTOR signaling, which regulates regenerative competence. Thus, these two pathways likely work in parallel to regulate injury signaling and regenerative competence, respectively, both of which are required for a regenerative outcome (Fig. 11C).

## Discussion

While DLK, and to a lesser extent LZK, have been studied in various models of neuronal injury in optic and sciatic nerves (Shin et al., 2012; Watkins et al., 2013; Welsbie et al., 2013, 2017), the present study investigates for the first time the role of DLK and LZK in axonal repair in the mammalian spinal cord. Using two injury models, we took a systematic approach to assess the effects of inducible DLK and LZK deletion on the regeneration and sprouting of CST axons. We found that co-deletion of DLK and LZK abolished CST regeneration and sprouting that are normally induced by PTEN deletion. Furthermore, co-deletion of DLK and LZK suppressed spontaneous CST sprouting to below wild-type levels. Deleting DLK and LZK did not interfere with PTEN deletion-induced activation of mTOR or the accompanying cellular hypertrophy; conversely, deleting PTEN did not noticeably affect the expression of DLK mRNA within Layer V of the cortex. These data demonstrate the critical role of neuronal DLK and LZK in axonal repair including both regeneration and sprouting in the mammalian spinal cord. The relative contribution of DLK versus LZK in CST regeneration appears to mirror that in RGC death (Welsbie et al., 2017). DLK/LZK-dependent injury signaling and PTEN/mTOR-dependent regenerative

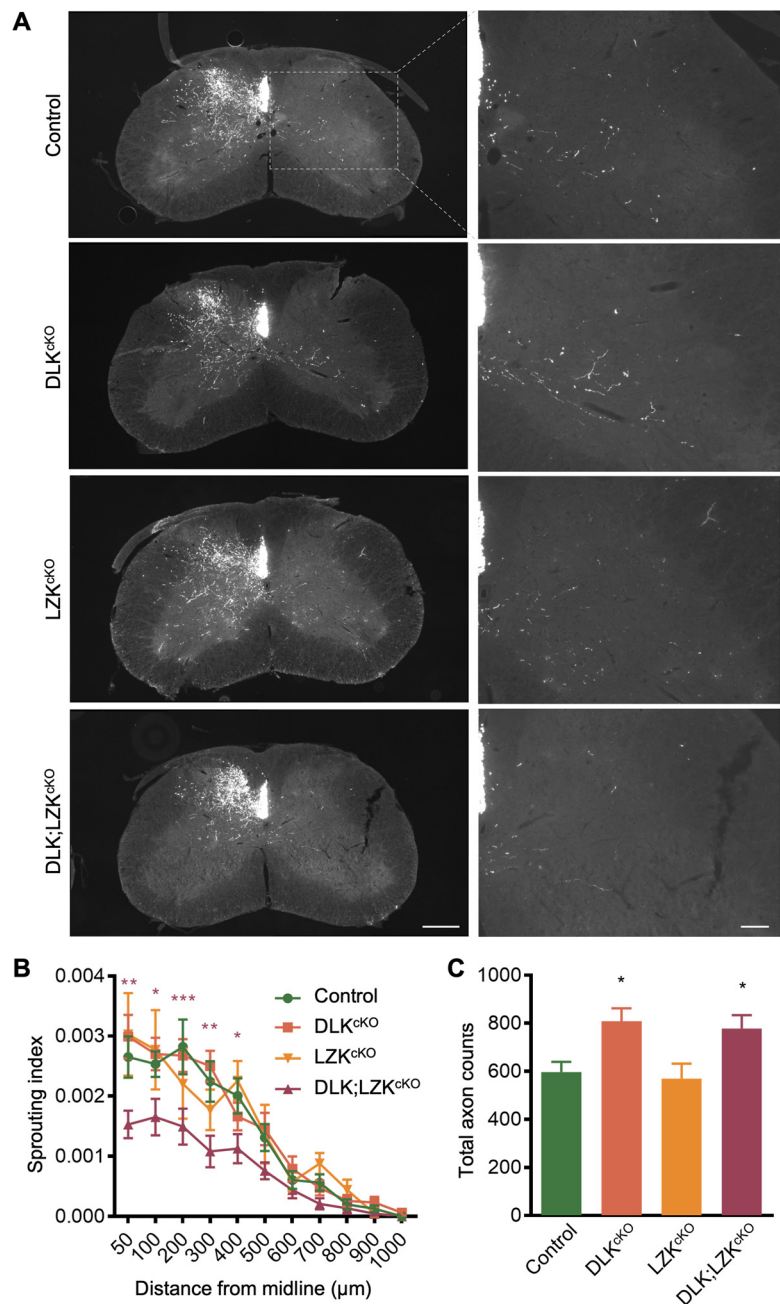


**Figure 10.** Deletion of both DLK and LZK, but not either kinase alone, reduces spontaneous CST sprouting to below wild-type levels. **A**, Representative images of BDA tracing of CST axons (white) on transverse cervical spinal cord sections from control, DLK<sup>ckO</sup>, LZK<sup>ckO</sup>, and DLK;LZK<sup>ckO</sup> mice. Scale bar: 300 μm (left panels), 100 μm (right panels). **B**, Quantification of CST sprouting across all four genotypes.  $N = 15$  (Control), 11 (DLK<sup>ckO</sup>), 8 (LZK<sup>ckO</sup>), 10 (DLK;LZK<sup>ckO</sup>). Two-way RM ANOVA revealed significant differences across genetic conditions ( $F_{(3,40)} = 3.708$ ,  $p = 0.0191$ ). Bonferroni *post hoc* test for multiple comparisons revealed that DLK;LZK<sup>ckO</sup> mice had significantly fewer axons than controls at 50 μm,  $p = 0.0055$ ; at 100 μm,  $p = 0.0423$ ; at 200 μm,  $p = 0.0007$ ; at 300 μm,  $p = 0.0036$ ; at 400 μm,  $p = 0.0431$ . \* $p < 0.05$ , \*\* $p < 0.01$ , \*\*\* $p < 0.001$ , \*\*\*\* $p < 0.0001$ . **C**, One-way ANOVA revealed significant differences of axon labeling at the level of medullas ( $F_{(3,40)} = 5.352$ ,  $p = 0.0034$ ). Specifically, DLK<sup>ckO</sup> and DLK;LZK<sup>ckO</sup> mice had higher labeling than controls ( $p = 0.0100$  and  $0.0368$ , respectively).

competence are likely independently controlled parallel processes, both of which are required for regeneration. Finally, together with our previous report implicating LZK in mediating astrogliosis and scar formation (Chen et al., 2018), the current study illustrates an emerging theme that the same signaling pathway such as the one involving DLK and LZK can function simultaneously in multiple cell types in the multicellular response to CNS injury.



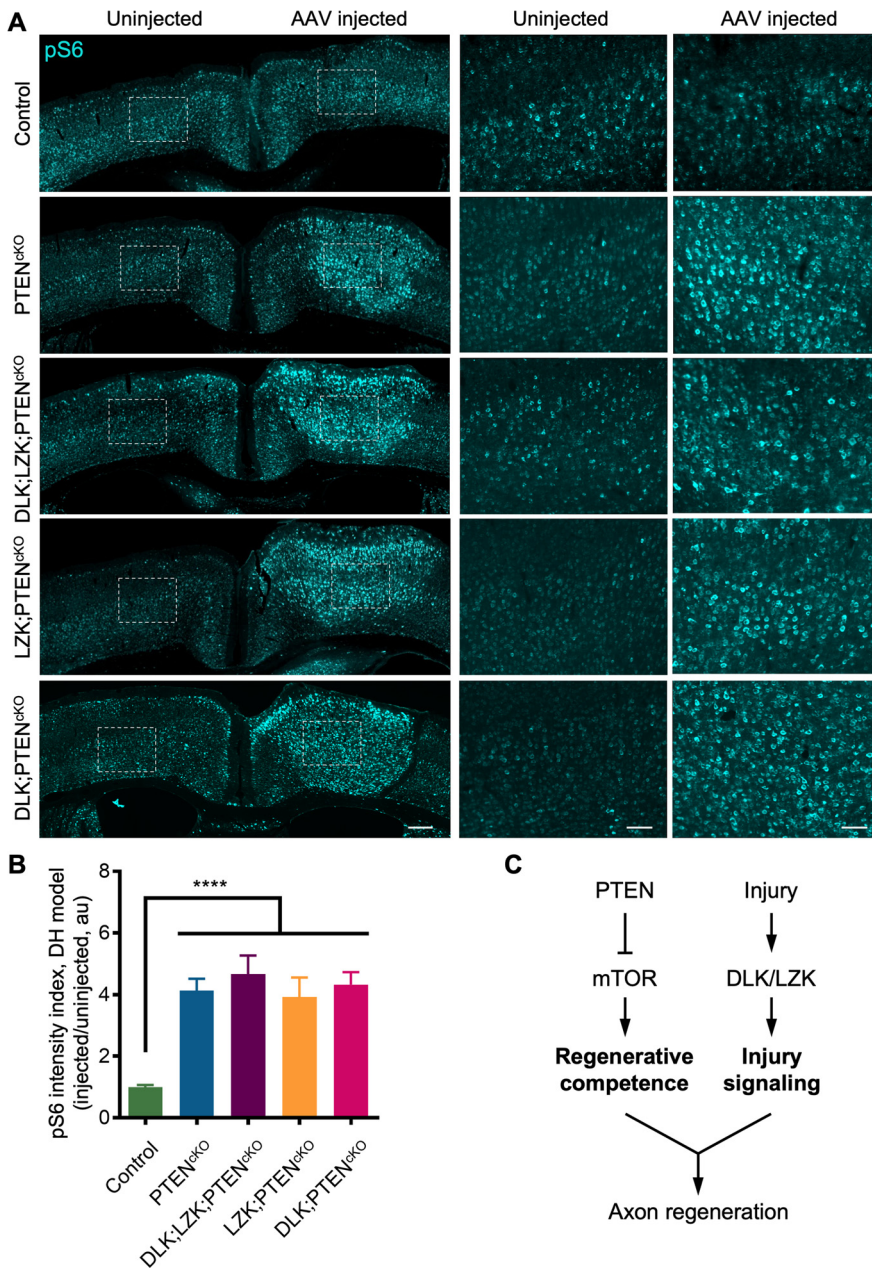


**Figure 11.** DLK and LZK deletion does not interfere with PTEN deletion-induced elevation of mTOR activity as assessed with pS6 in the dorsal hemisection injury model. **A**, Coronal brain sections of control, PTEN<sup>ck0</sup>, DLK;LZK;PTEN<sup>ck0</sup>, LZK;PTEN<sup>ck0</sup>, and DLK;PTEN<sup>ck0</sup> mice stained for pS6 after dorsal hemisection injury. Middle and right panels are higher magnification images of boxed areas in the left panels from the two hemispheres. AAV-GFP was injected into control mice; all other mice were injected with AAV-Cre. Scale bar: 300 μm (left panels, taken with 10× objective), 100 μm (middle and right panels, taken with 20× objective). **B**, Quantification of pS6 signals in mice that underwent dorsal hemisection injury, calculated as the ratio of pS6 signals in the AAV-injected hemisphere against the uninjected hemisphere. One-way ANOVA revealed significant differences across genetic conditions on pS6 staining ( $F_{(4,74)} = 18.58, p < 0.0001$ ). Multiple comparisons test with Bonferroni correction revealed significant elevations of pS6 signals compared with controls in PTEN<sup>ck0</sup>, DLK;LZK;PTEN<sup>ck0</sup>, LZK;PTEN<sup>ck0</sup>, and DLK;PTEN<sup>ck0</sup> (\*\*\*\* $p < 0.0001$  for each comparison). **C**, Proposed working model depicting DLK/LZK-mediated injury signaling and PTEN/mTOR-mediated regenerative competence as two parallel processes both of which are required to feed into a common regenerative program to produce a regenerative outcome.

Following axonal injury, neurons can initiate an array of cellular responses. DLK has been reported to mediate three such responses including proximal axon regeneration, distal axon degeneration, and cell death following optic or peripheral nerve injury (Miller et al., 2009; Shin et al., 2012; Watkins et al., 2013; Welsbie et al., 2013). In the retinal system, an optic nerve injury

triggers widespread (~80%) RGC death. Single gene deletion of DLK but not LZK partially protects against RGC death (Welsbie et al., 2013), while double deletion of both LZK and DLK provides additional protection (Welsbie et al., 2017). In addition to mediating RGC death after optic nerve injury, DLK is also required for PTEN deletion-induced retinal axon regeneration; accordingly, DLK regulates both the regenerative and apoptotic pathways following pathologic challenges (Watkins et al., 2013). After peripheral nerve injury, DLK deletion reduces distal Wallerian axon degeneration and proximal axon regeneration (Miller et al., 2009; Shin et al., 2012). At present, it is not known whether these divergent neuronal responses mediated by DLK/LZK are a function of neuronal types, injury models, and/or other cellular state variables such as PTEN/mTOR signaling. Nevertheless, in both CST regeneration (in the current study) and RGC death (Welsbie et al., 2017) following axonal injury, DLK appears to play a more prominent role, as deleting DLK, but not LZK, partially reduced regeneration or cell death; meanwhile, LZK further contributes to these processes as DLK and LZK double deletion produced a stronger phenotype than DLK deletion alone. On the other hand, DLK and LZK appear to be completely functionally redundant in both induced and spontaneous CST sprouting as deleting either kinase had no detectable effect. A recent report suggests that DLK and LZK are similarly functionally redundant in mediating RGC death in a mouse model of diffuse traumatic brain injury (Welsbie et al., 2019). Thus, the mammalian DLK and LZK function intrinsically in neurons to regulate divergent outcomes, as we have now shown for CST regeneration and sprouting in the spinal cord, with partial or full functional redundancy between the two kinases in a context-dependent manner.

A surprising result from the current study is that DLK and LZK co-regulate both PTEN deletion-induced sprouting and spontaneous sprouting in otherwise wild-type mice. In the literature,

DLK is studied extensively for its role in sensing neuronal stress and injury (Asghari Adib et al., 2018). By definition, sprouting is a response of uninjured neurons to a CNS injury elsewhere. It is conceivable that DLK/LZK-dependent injury signaling may only occur in injured neurons, and consequently would not be

expected to regulate axonal sprouting from uninjured neurons. However, our present study clearly showed that co-deletion of DLK and LZK blocks both spontaneous and PTEN deletion-induced sprouting following CNS injury. Uninjured neurons respond to an injury elsewhere cell non-autonomously to initiate compensatory sprouting. Thus, our data suggest that DLK/LZK-mediated injury signaling also occurs in neurons that are not physically damaged themselves but nevertheless sense an injury sustained by other neurons. The denervated neural tissue may secrete diffusible factors (e.g., cytokines, inflammatory signals) that trigger an injury response, akin to a secondary injury response, in sprouting and initially spared neurons. A recent study indicates that injury signals may spread to uninjured “bystander” neurons through a Draper/MEGF10-dependent mechanism mediated by glial cells (Hsu et al., 2021). Further studies are required to identify the exact mechanisms by which injury signals propagate to uninjured neurons to elicit axonal sprouting. In a mouse model of stroke, shRNA knock-down of C-C chemokine receptor 5 (CCR5) enhances motor recovery in an DLK-dependent manner that is accompanied by increased axonal sprouting (Joy et al., 2019). While not directly explored in the present study, we cannot exclude the possibility that DLK may also function beyond its role as a neuronal stress sensor. During development, DLK is involved with growth cone formation in growing axons; as development terminates, the activity of DLK is drastically downregulated by PHR E3 ubiquitin ligase activity (Nakata et al., 2005; Feoktistov and Herman, 2016; Borgen et al., 2017; Lewcock et al., 2007). It is possible that DLK (and LZK) signaling may reprise the role of modulating activity of proteins involved with cytoskeletal elements during axonal repair (Ghosh-Roy et al., 2012; Karney-Grobe et al., 2018), providing an alternative explanation for its (their) involvement in axonal sprouting from uninjured neurons. Finally, although it is less likely, we cannot exclude an additional role for DLK and LZK in injured corticospinal neurons to elicit sprouting from uninjured neurons. In this scenario, DLK and LZK in the degenerating axons caudal to the unilateral pyramidotomy would signal across the midline in the cervical cord to induce CST sprouting from the uninjured side. Testing this scenario would require DLK and LZK gene deletion in injured corticospinal neurons, rather than in uninjured neurons as was performed in the current study.

How does co-deletion of DLK and LZK block PTEN deletion-induced CST regeneration and sprouting? A previous study with the optic nerve injury model indicates that DLK mediates a majority of the injury-induced gene expression changes (Watkins et al., 2013). While similar expression profiling on corticospinal neurons under various genetic conditions remain to be conducted, we found that mTOR activity is still robust in

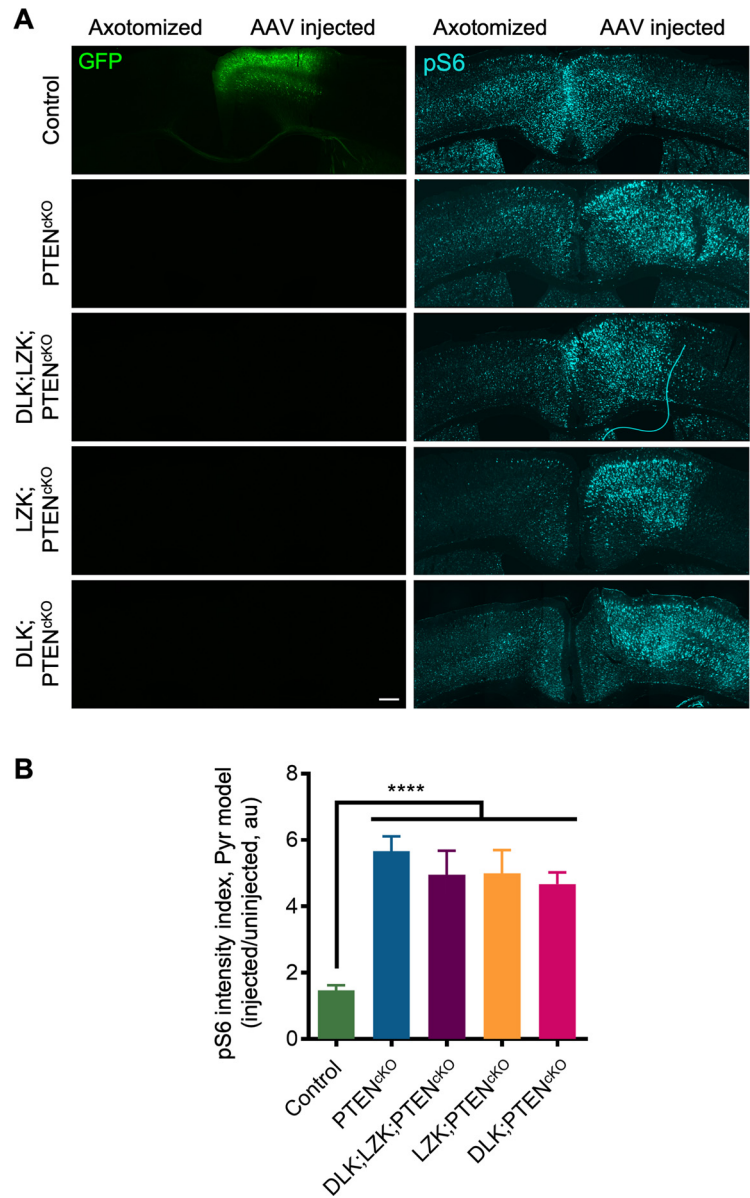


**Figure 12.** DLK and LZK deletion does not interfere with PTEN deletion-induced elevation of mTOR activity as assessed with pS6 in the unilateral pyramidotomy model. **A**, Representative images of coronal brain sections showing pS6 staining in mice that underwent unilateral pyramidotomy on one side (left) and AAV injection on the other side (right) of the brain. Similar to what was observed in the dorsal hemisection model, Cre injection, but not GFP injection, led to robust elevations in pS6 expression in mice that underwent Cre-mediated deletion of PTEN, regardless of DLK and/or LZK deletion. Scale bar: 300  $\mu$ m. **B**, Quantification of pS6 signals in mice that underwent pyramidotomy injury. One-way ANOVA revealed significant differences across genetic conditions on pS6 staining ( $F_{(4,107)} = 9.899$ , \*\*\*\* $p < 0.0001$ ). Multiple comparisons test with Bonferroni correction revealed significant elevations of pS6 signal compared with controls in PTEN<sup>ΔKO</sup>, DLK;LZK;PTEN<sup>ΔKO</sup>, LZK;PTEN<sup>ΔKO</sup>, and DLK;PTEN<sup>ΔKO</sup> ( $p < 0.0001$  for PTEN<sup>ΔKO</sup>, DLK;LZK;PTEN<sup>ΔKO</sup>, LZK;PTEN<sup>ΔKO</sup>, and  $p = 0.0010$  for DLK;PTEN<sup>ΔKO</sup>, respectively).

DLK;LZK;PTEN<sup>ΔKO</sup> mice. This result indicates that the DLK/LZK-dependent injury signaling process is not a prerequisite for PTEN/mTOR-dependent regenerative competence in a linear pathway. Rather, DLK/LZK signaling appears to function in parallel to PTEN/mTOR in promoting CST axonal repair. In the absence of DLK and LZK signaling, PTEN deletion still triggers a pro-growth mTOR pathway, but this elevated regenerative competence (or potential) fails to translate into a regenerative outcome. Both injury signaling and regenerative competence must feed into a regenerative program coincidentally for regeneration to occur (Fig. 11C).



Ultimately, the ability for the CNS to respond to an injury relies on a wide array of cellular types, ranging from microglia that act as first responders, astrocytes that undergo reactive transformation, macrophages and fibroblasts that occupy the lesion core, to uninjured and injured neurons that exhibit a variety of injury responses. The field of CNS regeneration has traditionally categorized molecular pathways into neuron-intrinsic versus extrinsic ones. Together with published data, our current study supports the notion that the same signaling pathway may act both neuron-intrinsically and extrinsically to regulate the multicellular response to CNS injury. Our previous study identified LZK as a critical regulator of astrogliosis and scar formation after spinal cord injury (Chen et al., 2018). The current study indicates that neuronal LZK and DLK together play important roles in CST regeneration and sprouting in the mammalian spinal cord. Thus, the same DLK/LZK signaling pathway may simultaneously act in neurons and astrocytes to regulate the neuronal and astrocytic responses to injury, respectively, in the mammalian spinal cord. In this regard, a caveat of the current study is that while our AAV2 vectors predominantly infect neurons over astrocytes (Haery et al., 2019), we cannot exclude a small effect through their infection of brain astrocytes around the AAV injection site. However, we anticipate that any astrocytic impact on CST axon regeneration would likely be more prominent at the spinal cord injury site where regenerating axons navigate the injured CNS environment as compared with the brain AAV injection site where their somas reside. The DLK/LZK pathway joins the SOCS3/STAT3 pathway (Okada et al., 2006; Herrmann et al., 2008; Smith et al., 2009; Jin et al., 2015) as dual regulators of axonal repair and astrocytic scarring in neurons and astrocytes, respectively. In addition, there is gain of function data implicating a third regeneration pathway, PTEN/mTOR, in astroglial scarring (Chen et al., 2016). Indeed, the multicellular role of DLK/LZK may not be restricted to neurons and astrocytes. Recent studies indicate that loss of DLK alters the microglia phenotype under pathologic condition (Le Pichon et al., 2017; Wlaschin et al., 2018), although whether DLK acts cell autonomously in microglia in those studies is not known.

Future studies will be required to understand the downstream mediators of neuronal DLK and LZK in regulating axonal repair, their context-dependent roles in different injury outcomes (e.g., regeneration vs cell death), and how the two kinases coordinate the multicellular responses to spinal cord injury. For example, transcriptomic profiling at different time points after injury coupled with genetic manipulation of the two kinases may reveal insights on downstream transcriptional programs that mediate their effect on regeneration. Unlike optic nerve crush that causes substantial RGC death, spinal cord injury typically does not lead to significant corticospinal neuron death (Nielson et al., 2010, 2011). Thus, a subcortical lesion model where the injury occurs much closer to the cell bodies (Giehl and Tetzlaff, 1996; Hollis et al., 2009) will be required to assess the role of DLK and LZK in axotomy-induced corticospinal neuron death. In addition to a direct role of neuronal DLK and LZK in regulating axonal repair, astrocytic LZK (and possibly DLK) may also indirectly regulate axonal repair through their effect on the astrocyte response and scar formation at and near the injury site, which can be examined with astrocyte-specific gene manipulations. Finally, whether DLK and LZK mediate distal (Wallerian) axon degeneration and how that might interact with the regeneration of proximal axonal segments after spinal cord injury remain interesting questions. Understanding these questions may help design new

therapeutic strategies aimed at improving outcomes for patients with spinal cord injury.

## References

- Asghari Adib E, Smithson LJ, Collins CA (2018) An axonal stress response pathway: degenerative and regenerative signaling by DLK. *Curr Opin Neurobiol* 53:110–119.
- Angeli CA, Edgerton VR, Gerasimenko YP, Harkema SJ (2014) Altering spinal cord excitability enables voluntary movements after chronic complete paralysis in humans. *Brain* 137:1394–1409.
- Bareyre FM, Kerschensteiner M, Raineteau O, Mettenleiter TC, Weinmann O, Schwab ME (2004) The injured spinal cord spontaneously forms a new intraspinal circuit in adult rats. *Nat Neurosci* 7:269–277.
- Borgen MA, Wang D, Grill B (2017) RPM-1 regulates axon termination by affecting growth cone collapse and microtubule stability. *Development* 144:4658–4672.
- Chang L, Karin M (2001) Mammalian MAP kinase signalling cascades. *Nature* 410:37–40.
- Chen M, Geoffroy CG, Wong HN, Tress O, Nguyen MT, Holzman LB, Jin Y, Zheng B (2016) Leucine zipper-bearing kinase promotes axon growth in mammalian central nervous system neurons. *Sci Rep* 6:31482.
- Chen M, Geoffroy CG, Meves JM, Narang A, Li Y, Nguyen MT, Khai VS, Kong X, Steinke CL, Carolino KI, Elzière L, Goldberg MP, Jin Y, Zheng B (2018) Leucine zipper-bearing kinase is a critical regulator of astrocyte reactivity in the adult mammalian CNS. *Cell Rep* 22:3587–3597.
- Collins CA, Wairkar YP, Johnson SL, DiAntonio A (2006) Highwire restrains synaptic growth by attenuating a MAP kinase signal. *Neuron* 51:57–69.
- Feoktistov AI, Herman TG (2016) Wallenda/DLK protein levels are temporally downregulated by Tramtrack69 to allow R7 growth cones to become stationary boutons. *Development* 143:2983–2993.
- Gallent EA, Steward O (2018) Neuronal PTEN deletion in adult cortical neurons triggers progressive growth of cell bodies, dendrites, and axons. *Exp Neurol* 303:12–28.
- Geoffroy CG, Zheng B (2014) Myelin-associated inhibitors in axonal growth after CNS injury. *Curr Opin Neurobiol* 27:31–38.
- Geoffroy CG, Lorenzana AO, Kwan JP, Lin K, Ghassemi O, Ma A, Xu N, Creger D, Liu K, He Z, Zheng B (2015) Effects of PTEN and Nogo codeletion on corticospinal axon sprouting and regeneration in mice. *J Neurosci* 35:6413–6428.
- Ghosh-Roy A, Goncharov A, Jin Y, Chisholm AD (2012) Kinesin-13 and Tubulin posttranslational modifications regulate microtubule growth in axon regeneration. *Dev Cell* 23:716–728.
- Giehl K, Tetzlaff W (1996) BDNF and NT-3, but not NGF, prevent axotomy-induced death of rat corticospinal neurons in vivo. *Eur J Neurosci* 8:1167–1175.
- Gutilla EA, Buyukozturk MM, Steward O (2016) Long-term consequences of conditional genetic deletion of PTEN in sensorimotor cortex of neonatal mice. *Exp Neurol* 279:27–39.
- Haery L, Deverman BE, Matho KS, Cetin A, Woodard K, Cepko C, Guerin KI, Rego MA, Ersing I, Bachle SM, Kamens J, Fan M (2019) Adeno-associated virus technologies and methods for targeted neuronal manipulation. *Front Neuroanat* 13:93.
- Hammarlund M, Nix P, Hauth L, Jorgensen EM, Bastiani M (2009) Axon regeneration requires a conserved MAP kinase pathway. *Science* 323:802–806.
- He Z, Jin Y (2016) Intrinsic control of axon regeneration. *Neuron* 90:437–451.
- Herrmann JE, Imura T, Song B, Qi J, Ao Y, Nguyen TK, Korsak RA, Takeda K, Akira S, Sofroniew MV (2008) STAT3 is a critical regulator of astrogliosis and scar formation after spinal cord injury. *J Neurosci* 28:7231–7243.
- Hollis ER, Lu P, Blesch A, Tuszynski MH (2009) IGF-I gene delivery promotes corticospinal neuronal survival but not regeneration after adult CNS injury. *Exp Neurol* 215:53–59.
- Holzman LB, Merritt SE, Fan G (1994) Identification, molecular cloning, and characterization of dual leucine zipper bearing kinase. A novel serine/threonine protein kinase that defines a second subfamily of mixed lineage kinases. *J Biol Chem* 269:30808–30817.
- Hsu JM, Kang Y, Corty MM, Mathieson D, Peters OM, Freeman MR (2021) Injury-induced inhibition of bystander neurons requires dSarm and signaling from glia. *Neuron* 109:473–487.e5.



- Jin D, Liu Y, Sun F, Wang X, Liu X, He Z (2015) Restoration of skilled locomotion by sprouting corticospinal axons induced by co-deletion of PTEN and SOCS3. *Nat Commun* 6:8074.
- Jin Y, Zheng B (2019) Multitasking: dual leucine zipper-bearing kinases in neuronal development and stress management. *Annu Rev Cell Dev Biol* 35:501–521.
- Joy MT, Ben Assayag E, Shabashov-Stone D, Liraz-Zaltsman S, Mazzitelli J, Arenas M, Abduljawad N, Kliper E, Korczyn AD, Thareja NS, Kesner EL, Zhou M, Huang S, Silva TK, Katz N, Bornstein NM, Silva AJ, Shohami E, Carmichael ST (2019) CCR5 is a therapeutic target for recovery after stroke and traumatic brain injury. *Cell* 176:1143–1157.e13.
- Karney-Grobe S, Russo A, Frey E, Milbrandt J, DiAntonio A (2018) HSP90 is a chaperone for DLK and is required for axon injury signaling. *Proc Natl Acad Sci U S A* 115:E9899–E9908.
- Le Pichon CE, et al. (2017) Loss of dual leucine zipper kinase signaling is protective in animal models of neurodegenerative disease. *Sci Transl Med* 9:eaag0394.
- Lee JK, Geoffroy CG, Chan AF, Tolentino KE, Crawford MJ, Leal MA, Kang B, Zheng B (2010) Assessing spinal axon regeneration and sprouting in Nogo-, MAG-, and OMgp-deficient mice. *Neuron* 66:663–670.
- Lewcock JW, Genoud N, Lettieri K, Pfaff SL (2007) The ubiquitin ligase Phr1 regulates axon outgrowth through modulation of microtubule dynamics. *Neuron* 56:604–620.
- Li Y, Ritchie EM, Steinke CL, Qi C, Chen L, Zheng B, Jin Y (2021) Activation of MAP3K DLK and LZK in Purkinje cells causes rapid and slow degeneration depending on signaling strength. *Elife* 10:e63509.
- Liu K, Lu Y, Lee JK, Samara R, Willenberg R, Sears-Kraxberger I, Tedeschi A, Park KK, Jin D, Cai B, Xu B, Connolly L, Steward O, Zheng B, He Z (2010) PTEN deletion enhances the regenerative ability of adult corticospinal neurons. *Nat Neurosci* 13:1075–1081.
- Lu P, Wang Y, Graham L, McHale K, Gao M, Wu D, Brock J, Blesch A, Rosenzweig ES, Havton LA, Zheng B, Conner JM, Marsala M, Tuszynski MH (2012) Long-distance growth and connectivity of neural stem cells after severe spinal cord injury. *Cell* 150:1264–1273.
- Lu Y, Belin S, He Z (2014) Signaling regulations of neuronal regenerative ability. *Curr Opin Neurobiol* 27:135–142.
- Miller BR, Press C, Daniels RW, Sasaki Y, Milbrandt J, DiAntonio A (2009) A dual leucine kinase-dependent axon self-destruction program promotes Wallerian degeneration. *Nat Neurosci* 12:387–389.
- Nakata K, Abrams B, Grill B, Goncharov A, Huang X, Chisholm AD, Jin Y (2005) Regulation of a DLK-1 and p38 MAP kinase pathway by the ubiquitin ligase RPM-1 is required for presynaptic development. *Cell* 120:407–420.
- Nielson JL, Sears-Kraxberger I, Strong MK, Wong JK, Willenberg R, Steward O (2010) Unexpected survival of neurons of origin of the pyramidal tract after spinal cord injury. *J Neurosci* 30:11516–11528.
- Nielson JL, Strong MK, Steward O (2011) A reassessment of whether cortical motor neurons die following spinal cord injury. *J Comp Neurol* 519:2852–2869.
- Okada S, Nakamura M, Katoh H, Miyao T, Shimazaki T, Ishii K, Yamane J, Yoshimura A, Iwamoto Y, Toyama Y, Okano H (2006) Conditional ablation of Stat3 or Socs3 discloses a dual role for reactive astrocytes after spinal cord injury. *Nat Med* 12:829–834.
- Park KK, Liu K, Hu Y, Smith PD, Wang C, Cai B, Xu B, Connolly L, Kramvis I, Sahin M, He Z (2008) Promoting axon regeneration in the adult CNS by modulation of the PTEN/mTOR pathway. *Science* 322:963–966.
- Sakuma H, Ikeda A, Oka S, Kozutsumi Y, Zanetta JP, Kawasaki T (1997) Molecular cloning and functional expression of a cDNA encoding a new member of mixed lineage protein kinase from human brain. *J Biol Chem* 272:28622–28629.
- Shin JE, Cho Y, Beirowski B, Milbrandt J, Cavalli V, DiAntonio A (2012) Dual Leucine Zipper Kinase is required for retrograde injury signaling and axonal regeneration. *Neuron* 74:1015–1022.
- Silver J, Schwab ME, Popovich PG (2014) Central nervous system regenerative failure: role of oligodendrocytes, astrocytes, and microglia. *Cold Spring Harb Perspect Biol* 7:a020602.
- Smith PD, Sun F, Park KK, Cai B, Wang C, Kuwako K, Martinez-Carrasco I, Connolly L, He Z (2009) SOCS3 deletion promotes optic nerve regeneration in vivo. *Neuron* 64:617–623.
- Sofroniew MV (2018) Dissecting spinal cord regeneration perspective. *Nature* 557:343–350.
- Starkey ML, Barritt AW, Yip PK, Davies M, Hamers FPT, McMahon SB, Bradbury EJ (2005) Assessing behavioural function following a pyramidotomy lesion of the corticospinal tract in adult mice. *Exp Neurol* 195:524–539.
- Steward O, Willenberg R (2017) Rodent spinal cord injury models for studies of axon regeneration. *Exp Neurol* 287:374–383.
- Tedeschi A, Bradke F (2013) The DLK signalling pathway - a double-edged sword in neural development and regeneration. *EMBO Rep* 14:605–614.
- Tuszynski MH, Steward O (2012) Concepts and methods for the study of axonal regeneration in the CNS. *Neuron* 74:777–791.
- Ueno M, Hayano Y, Nakagawa H, Yamashita T (2012) Intraspinally rewiring of the corticospinal tract requires target-derived brain-derived neurotrophic factor and compensates lost function after brain injury. *Brain* 135:1253–1267.
- Watkins TA, Wang B, Huntwork-Rodriguez S, Yang J, Jiang Z, Eastham-Anderson J, Modrusan Z, Kaminker JS, Tessier-Lavigne M, Lewcock JW (2013) DLK initiates a transcriptional program that couples apoptotic and regenerative responses to axonal injury. *Proc Natl Acad Sci U S A* 110:4039–4044.
- Weidner N, Ner A, Salimi N, Tuszynski MH (2001) Spontaneous corticospinal axonal plasticity and functional recovery after adult central nervous system injury. *Proc Natl Acad Sci U S A* 98:3513–3518.
- Welsbie DS, et al. (2013) Functional genomic screening identifies dual leucine zipper kinase as a key mediator of retinal ganglion cell death. *Proc Natl Acad Sci U S A* 110:4045–4050.
- Welsbie DS, et al. (2017) Enhanced functional genomic screening identifies novel mediators of dual leucine zipper kinase-dependent injury signaling in neurons. *Neuron* 94:1142–1154.e6.
- Welsbie DS, Ziogas NK, Xu L, Kim BJ, Ge Y, Patel AK, Ryu J, Lehar M, Alexandris AS, Stewart N, Zack DJ, Koliatsos VE (2019) Targeted disruption of dual leucine zipper kinase and leucine zipper kinase promotes neuronal survival in a model of diffuse traumatic brain injury. *Mol Neurodegener* 14:44.
- Wlaschin JJ, Gluski JM, Nguyen E, Silberberg H, Thompson JH, Chesler AT, Le Pichon CE (2018) Dual leucine Zipper Kinase is required for mechanical allodynia and microgliosis after nerve injury. *Elife* 7:e33910.
- Xiong X, Wang X, Ewanek R, Bhat P, DiAntonio A, Collins CA (2010) Protein turnover of the Wallenda/DLK kinase regulates a retrograde response to axonal injury. *J Cell Biol* 191:211–223.
- Yan D, Jin Y (2012) Regulation of DLK-1 kinase activity by calcium-mediated dissociation from an inhibitory isoform. *Neuron* 76:534–548.
- Yan D, Wu Z, Chisholm AD, Jin Y (2009) The DLK-1 kinase promotes mRNA stability and local translation in *C. elegans* synapses and axon regeneration. *Cell* 138:1005–1018.